J. Fluid Mech. (2022), *vol*. 936, A22, doi:10.1017/jfm.2022.63

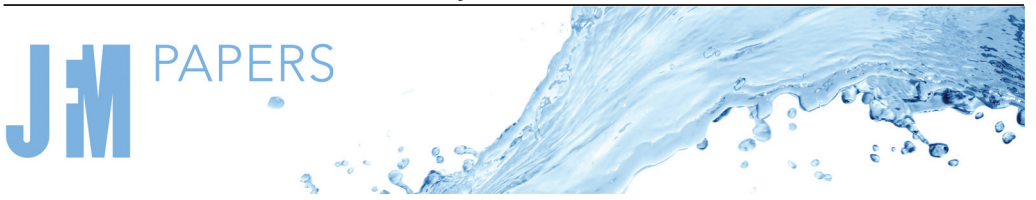

Theoretical analysis on the ignition of a combustible mixture by a hot particle

Dehai Yu[1] **and Zheng Chen**[1],†

[1]SKLTCS, CAPT, BIC-ESAT, Department of Mechanics and Engineering Science, College of Engineering, Peking University, Beijing 100871, PR China

(Received 25 July 2021; revised 30 October 2021; accepted 17 January 2022)

Mechanical spark is an important ignition source in various industrial processes involving combustible mixtures and it may cause serious safety issues. In this work, we analysed the ignition induced by hot particles in a combustible mixture. In Semenov's transient ignition criterion, we introduced a hypothetical heat loss coefficient accounting for the temperature inhomogeneity and obtained a revised ignition criterion which allows us to calculate the ignition delay time. Explicit expressions for the critical ignition temperature were derived and used to demonstrate the primary impacts of temperature inhomogeneity on the ignition process. Consistent with experimental and numerical results, the temperature inhomogeneity is intensified by either reducing the particle size or convective heat transfer at the particle surface, resulting in an increase of the critical ignition temperature. For flow separation on the particle surface, the boundary layer problem was solved based on a Blasius series. A temperature gradient for ignition was defined at the location of flow separation to reproduce the experimentally observed phenomenon that ignition prefers to occur first near the flow separation position. It is shown that the unsteadiness of particle cooling makes negligible contribution to the ignition process because of the exceedingly large density ratio between the particle and the ambient gas. In addition, the finite residence time of ignition for a fluid parcel due to its elevation from the particle surface leads to additional growth in the critical ignition temperature. However, such a correction appears to be inconsequential because the ignition of the fluid parcel restricted to the Frank–Kamenetskii region is close to the particle surface.

Key words: combustion

1. Introduction

In various industrial processes such as manufacturing and aviation, it is inevitable that small, hot particles are produced. Such hot particles are also known as mechanical

† Email address for correspondence: cz@pku.edu.cn

sparks since they usually glow because of the exceedingly high temperature (Hawksworth *et al.* 2005; Beyer & Markus 2012). The nature of the high temperature makes the mechanical spark an efficient ignition source. When a mechanical spark enters a flammable environment, the possibility of unwanted explosion due to ignition on the particle surface is substantially promoted (Eckhoff & Thomassen 1994; Hawksworth *et al.* 2005; Proust *et al.* 2007). Such accidental ignition and explosion can lead to tremendous damage and hazards. Besides, hot particle induced ignition is one of the important pathways to wildland and urban spot fires (Wang *et al.* 2016; Urban 2017; Urban *et al.* 2017). Therefore, an in-depth understanding of the underlying physics behind hot particle induced ignition is of crucial importance for industrial and fire safety.

The ignition of a combustible mixture by a mechanical spark takes place close to the hot surface (Law 2010). Such an ignition process is essentially inhomogeneous since there is large temperature gradient around the hot particle. Stamatov, King & Zhang (2005) conducted experiments on the ignition of quiescent CH_4/air mixtures caused by a laser-heated particle. They showed that the ignition delay time depends on the equivalence ratio and has a minimum value for a stoichiometric mixture. Beyer & Markus (2012) investigated the ignition capability of inert particles in a static explosive mixture. Their experiments and simulations showed that reducing the particle size promotes the critical ignition temperature. Roth *et al.* (2014) considered the thermal ignition of a quiescent H_2/air mixture by a small hot particle whose diameter was in the range from 0.3 to 0.8 mm. Their experiments showed that the critical ignition temperature strongly depends on the material of the hot particle. However, such a phenomenon can hardly be reproduced in numerical simulation. It was hypothesized that the surface reaction, i.e. quenching and catalysis, might contribute to the large difference in the critical ignition temperatures corresponding to different materials. Roth, Häber & Bockhorn (2017) examined the ignition process of different fuel/air mixtures by a silicon nitride particle. They found that the critical ignition temperature varies widely among different fuels and increases consistently as the equivalence ratio approaches the ignition limit. Wang & Chen (2020) conducted transient one-dimensional simulations on the ignition of CH_4/air and H_2/air mixtures by an inert hot particle, and found that the ignition delay time strongly depends on the particle size. Besides, Wang *et al.* (2021) found that the low-temperature chemistry plays an important role in hot particle induced ignition.

In general, the creation of mechanical sparks by means of mechanical action at the solid surface is associated with a non-vanishing momentum of the hot particle. Therefore, in most situations, the hot particle moves relative to the explosive mixture, leading to convective heat transfer around the particle surface in addition to pure heat conduction under quiescent conditions. Coronel *et al.* (2016, 2018) used a novel experimental set-up in observing the ignition of n-hexane/air mixture by a moving hot particle. Implementing a shear interferometer, they visualized the ignition kernel formation and the subsequent flame propagation. Melguizo-Gavilanes *et al.* (2016, 2017*a*,*b*) conducted a series of two-dimensional simulations on ignition induced by a hot particle falling into a combustible mixture. They observed that the boundary layer development and flow separation have crucial impacts on the ignition process, which is consistent with the experimental results of Mével *et al.* (2016, 2019). Usually, ignition occurs between the front stagnation point and the location of flow separation, and the ignition position moves downstream as the particle temperature decreases. In particular, ignition first takes place adjacent to the separation point when the particle temperature is close to the threshold value. Zirwes *et al.* (2019) revisited the ignition of a combustible mixture by

a moving hot particle based on both two-dimensional (2-D) and 3-D simulations. An in-depth understanding was obtained concerning the dependence of the critical ignition temperature on the relative velocity, ranging from creeping flow to flow with unsteady vortex shedding. They showed that a 2-D simulation assuming axisymmetric flow agrees well with a 3-D simulation in predicting the critical ignition temperature for relatively small velocities. However, the deviation becomes noticeable at higher flow velocities due to the 3-D unsteady vortices appearing behind the hot particle.

Ignition of a combustible mixture by a hot particle can be considered as the particular situation of ignition by a hot surface (Law 2010). Concerning thermal ignition of methane/air mixtures by a hot surface, Laurendeau (1982) developed a simple scaling correlation among particle temperature, size, pressure and flow velocity, using van't Hoff's ignition criterion. However, the temperature inhomogeneity was not fully considered in his work. The temperature inhomogeneity is represented by its gradient adjacent to the particle surface, whose magnitude is dominated by the local curvature. Law (1978*a*,*b*, 1979) conducted a large activation energy asymptotic analysis for hot particle induced ignition in a quiescent reactive mixture and obtained the ignition criterion in terms of a reduced Damköhler number, which interpreted the thermal energy balance between heat release from chemical reaction and heat loss due to conduction in steady state. Su & Sirignano (1981) revisited the same problem and in their asymptotic analysis, the second-order correction terms were retained for both temperature and mass fraction of the reactive species. Compared with a transient calculation (Su, Homan & Sirignano 1979), the second-order solution provided an improved ignition criterion. Based on the consideration that the ignition process was minimally affected by the geometry of the body, Law (1979) analysed the transient ignition of a combustible exposed to hot isothermal bodies. The flow field adjacent to the surface was shown to be diffusive–reactive in nature and satisfied local similarity, which enables the derivation of an explicit expression for the ignition delay time, denoted by τ_{ig}. However, at moderate to large Reynolds numbers, the flow separates at the rear hemisphere of the particle, and moreover the flow field before separation does not satisfy self-similarity. Consequently, the explicit analytical description of the velocity profile becomes unavailable (Johnson & Patel 1999; Schlichting & Gersten 2016). This imposes further difficulty in analytically solving temperature inhomogeneity at the particle surface due to convection (Riley 1986; Paterson & Hayhurst 2000).

Ignition is essentially a transient process involving multiple time scales. Ignition is characterized by the appearance of sustained combustion, where the rate of heat release due to chemical reaction is balanced by the rate of heat loss. For ignition by a hot particle with constant temperature in a quiescent mixture, the heat loss can be solely attributed to the temperature inhomogeneity at the particle surface. The critical ignition condition defines the largest rate of heat loss that can support combustion in the limit situation of steady state, i.e. $\tau_{ig} \to \infty$, and accordingly, the critical ignition temperature can be derived.

The relative motion between the hot particle and the combustible mixture introduces additional transient effects during the ignition process. On the one hand, the enhanced heat transfer resulting from both conduction and convection on the particle surface may shorten the cooling time (denoted by τ_{pc}) of the hot particle (Leal 2007). On the other hand, ignition takes place at some distance from the hot surface, implying that the fluid parcel where ignition first occurs has a finite residence time (denoted by τ_{res}) adjacent to the hot particle (Melguizo-Gavilanes *et al.* 2016, 2017*a*; Mével *et al.* 2016). The time scales τ_{pc} and τ_{res} introduce transient effects to the ignition process. Under such situations, the critical

ignition condition is revised to the equality of the ignition delay time and the characteristic time of the corresponding unsteady process, e.g. $\tau_{ig} = \tau_{pc}$ or $\tau_{ig} = \tau_{res}$. In comparison with steady state situations, we hypothesize that the finiteness of τ_{pc} and τ_{res} may increase the critical ignition temperature. Coronel (2016) proposed a simplified ignition model in which the relevant time scales were discussed in the scaling sense. However, quantitative comparison among these time scales was not conducted.

Based on the above-mentioned considerations, this work aims to develop a theoretical model for the ignition of a combustible mixture by a hot spherical particle. The present model can quantitatively interpret the role of temperature inhomogeneity and various transient effects on ignition behaviour and provide the dependence of the critical ignition temperature on relevant parameters in explicit form, which is so far not in place. The remaining parts of this paper proceed as follows. In § 2, Semenov's transient ignition criterion is revised by introducing a hypothetical volumetric heat loss to account for the temperature inhomogeneity, and accordingly, the ignition delay time can be evaluated analytically. In § 3, an in-depth discussion is presented on the effect of temperature inhomogeneity, resulting from both conductive and convective heat transfer, on the hot particle induced ignition process. An explicit formula for the critical ignition temperature, interpreting its dependence upon various affecting parameters, is derived. In § 4, the transient effect due to particle cooling is discussed. The particle cooling time is determined by solving the thermal energy equation of the solid particle and is compared with the τ_{ig} obtained in § 2. In § 5, the transient effect due to the motion of the ignition fluid parcel is taken into account, and its contribution to the change of critical ignition temperature is assessed. The general conclusions are given in § 6.

2. The inhomogeneous ignition criterion

Discharging a hot particle into a combustible mixture can lead to ignition. According to thermal ignition theory, ignition is most likely to take place first on the particle surface, where the temperature is highest. In addition to thermal runaway, ignition is also controlled by complicated chemical reaction pathways. The active radicals, e.g. H and OH, can be destroyed due to collision with the particle surface (Glassman, Yetter & Glumac 2014). Therefore, the fluid parcel, where ignition occurs first, should be slightly elevated from the solid surface such that its temperature is almost identical to that of the particle and meanwhile the accumulation of radicals exceeds termination. This fact was found in previous simulations by Melguizo-Gavilanes *et al.* (2017*b*).

The hot particle continuously transfers thermal energy into the relatively cool ambient gas, leading to large temperature gradient in the vicinity of the particle surface. Pertaining to such inhomogeneous ignition process, Law (1978*a*) analysed the hot particle induced ignition in the absence of relative motion between the particle and the environmental gas, and the temperature of the particle was assumed constant. The diffusive–reactive nature of the ignition process was analysed via large activation energy asymptotics. Adopting a simplified one-order Arrhenius-type model, the chemical reaction rate is

$$\omega = Bc_{F0} \exp(-T_a/T_s), \tag{2.1}$$

where B represents the reaction frequency factor, T_a the activation temperature, T_s the particle temperature and c_{F0} the fuel concentration in the mixture. The balance of heat release from chemical reaction and the heat loss due to temperature inhomogeneity gives the critical ignition condition, which is indicated by the following reduced Damköhler

number (Law 2010)

$$\Delta_I = \frac{2R_0^2 B\rho_g c_{pg}(T_{ad} - T_\infty)\exp(-T_a/T_s)}{\lambda_g T_a(1 - T_\infty/T_s)^2(\mathrm{d}\theta/\mathrm{d}\tilde{r})^2_{\tilde{r}=1}} \geq 1, \tag{2.2}$$

where λ_g, ρ_g and c_{pg} are respectively the thermal conductivity, density and the heat capacity of the combustible gaseous mixture, R_0 is the radius of the spherical particle, T_{ad} is the adiabatic flame temperature, T_∞ is the temperature of combustible mixture and $\theta = (T - T_\infty)/(T_s - T_\infty)$ is the normalized temperature. The normalized radial coordinate is defined by $\tilde{r} = r/R_0$. The term $(\mathrm{d}\theta/\mathrm{d}\tilde{r})_{\tilde{r}=1}$ denotes the non-dimensional temperature gradient on the particle surface, and it depends on the geometry of the particle. For a spherical particle in a quiescent frozen mixture, we have $(\mathrm{d}\theta/\mathrm{d}\tilde{r})_{\tilde{r}=1} = -1$, which will be shown in § 3.1.

The modified Damköhler number, given by (2.2), is a general formula that interprets the ignition of a quiescent combustible mixture close to the hot surface of a spherical particle of constant and uniform temperature. To derive (2.2) from first principles, the non-dimensional temperature is defined as $\tilde{T} = c_p T/q_c$, where q_c is the heat release from a unit mass of reactant mixture. According to the energy conservation law and the definition of the adiabatic flame temperature T_{ad}, we have $c_p(T_{ad} - T_\infty) = q_c$, which is substituted into the non-dimensional temperature and results in the appearance of T_{ad} in the modified Damköhler number.

The condition of $\Delta_I = 1$ gives the critical ignition temperature of the particle, T_{cr}, below which ignition fails since the heat generation from chemical reaction cannot compete with the heat loss to the ambient gas.

Fixing the frame of reference at the centre of the spherical particle, the relative motion between particle and combustible mixture can be equivalently regarded as the uniform flow of the environmental gas. Such relative motion between the combustible mixture and the hot particle modifies the ignition behaviour in three aspects. First, the convection accelerates heat transfer from the hot particle to the surrounding mixture and thus intensifies the temperature inhomogeneity at the particle surface. Second, the enhanced heat transfer facilitates the cooling of the hot particle, which leads to a decrease of the particle temperature. Last but not least, the fluid parcel where ignition occurs has finite residence time close to the hot particle, after which the fluid parcel cools down as it moves downstream. The steady state ignition criterion (Law 1978*a*,*b*, 2010) considers rigorously the non-homogeneous temperature profile in a quiescent environment and can predict the ignitability of the reactant gas subject to a hot particle with constant temperature. However, it meets exceeding difficulty in describing the temperature inhomogeneity caused by convective heat transfer because the velocity profiles adjacent to the particle surface may not be obtained in a mathematically explicit form. Consequently, the energy equation for the combustible mixture cannot be converted into the conventional conductive–reactive type, and the derivation route leading to (2.2) becomes inaccessible. Besides, the steady ignition theory is unable to evaluate the ignition delay time. To account for the unsteady effect, an additional term involving temporal evolution of the temperature should be included in the energy equation, which escalates the mathematical complexity in obtaining an analytical solution.

From the perspective of a Lagrangian description of the flow, we may trace the history of the ignition fluid parcel (abbreviated as IFP hereinafter) which ignites first. Since the size of the IFP can be arbitrarily small, we may assume that it has uniform temperature. In addition, appropriate heat loss must be associated with the IFP to account for the

inhomogeneity of the temperature profile close to the particle surface. Therefore, we may equivalently regard ignition as a local, non-adiabatic thermal explosion within the IFP. It is recognized that the consumption of reactant species appears to be negligible prior to ignition (Law 1978*a*, 2010). Consequently, the ignition process is solely characterized by the following energy equation for the IFP:

$$\rho_g c_{vg} \frac{\mathrm{d}T_I}{\mathrm{d}t} = q_c B c_{F0} \exp(-T_a/T_I) - h(T_I - T_\infty), \tag{2.3}$$

where T_I represents the temperature of the IFP, c_v the heat capacity at constant volume, q_c the heat release per unit mass of the reactant and h the effective volumetric heat loss coefficient to be determined. Conventionally, the non-dimensional temperature is defined by

$$\tilde{T} = \rho_g c_{vg} T / q_c c_{F0}, \tag{2.4}$$

where c_{vg} is the heat capacity at constant volume and q_c the heat release per unit mass of reactant. According to energy conservation, we may correlate q_c with T_{ad} via $q_c c_{F0} = \rho_g c_{vg}(T_{ad} - T_\infty)$, and consequently, we may alternatively write $\tilde{T} = T/(T_{ad} - T_\infty)$. The characteristic time for chemical reaction can be defined in terms of the non-dimensional temperature of the particle,

$$\tau_{ch} = \frac{\tilde{T}_s^2 \exp(\tilde{T}_a/\tilde{T}_s)}{\tilde{T}_a B}. \tag{2.5}$$

The heat loss coefficient h can also be written in non-dimensional form,

$$\tilde{h} = \frac{h\tau_{ch}}{\rho_g c_{vg}} = \frac{h\tilde{T}_s^2 \exp(\tilde{T}_a/\tilde{T}_s)}{\rho_g c_{vg} \tilde{T}_a B}. \tag{2.6}$$

In terms of $\tilde{T}$ and $\tilde{h}$, we can write (2.3) in dimensionless form

$$\frac{\mathrm{d}\tilde{T}_I}{\mathrm{d}\tilde{t}} = \frac{\tilde{T}_s^2}{\tilde{T}_a} \exp\left[-\tilde{T}_a\left(\frac{1}{\tilde{T}_I} - \frac{1}{\tilde{T}_s}\right)\right] - \tilde{h}(\tilde{T}_I - \tilde{T}_\infty). \tag{2.7}$$

Since the IFP is close to the particle surface, we have $T_I \approx T_s$. Assuming that $\tilde{T}_a \gg \tilde{T}_I$, we can write an asymptotic series for the latter, i.e.

$$\tilde{T}_I = \tilde{T}_s + \epsilon\chi, \tag{2.8}$$

where $\epsilon = \tilde{T}_s^2/\tilde{T}_a \ll 1$ is a small parameter, and χ is the first-order perturbation to the non-dimensional temperature of the IFP. Substituting (2.8) into (2.7) and collecting terms of like powers of ϵ, we obtain:

The leading-order equation for $\tilde{T}_s$

$$\frac{\mathrm{d}\tilde{T}_s}{\mathrm{d}\tilde{t}} = -\tilde{h}(\tilde{T}_s - \tilde{T}_\infty). \tag{2.9}$$

The first-order equation for χ

$$\frac{\mathrm{d}\chi}{\mathrm{d}\tilde{t}} = e^{\chi} - \tilde{h}\chi. \tag{2.10}$$

The leading-order (2.9) demonstrates that the temperature of the IFP continues to decay due to volumetric heat loss characterized by $\tilde{h}$. However, the magnitude of the first-order

correction to the temperature χ, according to (2.10), is also affected by heat release from chemical reaction. For a sufficiently large heat loss coefficient $\tilde{h}$, (2.10) suggests that χ approaches a finite value in the limit of $\tilde{t} \to \infty$. In association with the decay of $\tilde{T}_s$ according to (2.9), ignition is prohibited. To achieve successful ignition, the heat loss rate must be bounded from above, which is characterized by the explosive increase of χ in the course of time (Law 2010). The condition that ensures successful ignition can be determined according to the Semenov ignition criterion as

$$\tilde{h} \leq e. \tag{2.11}$$

The equality, $\tilde{h} = e$, holds for the critical ignition condition, which should be equivalent to $\Delta_I = 1$ derived by rigorously considering temperature inhomogeneity in the steady state theory. The critical ignition condition defines the reference state, at which the ignition could occur after a sufficiently long time, or the heat release by chemical reaction is balanced by heat transfer to the surroundings during the whole ignition process. Physical plausibility suggests that the heat loss effect could be varied independently from the chemical reaction rate. We solve for the reaction frequency factor B from the condition $\Delta_I = 1$ in terms of $(\mathrm{d}\theta/\mathrm{d}\tilde{r})_{\tilde{r}=1}$ using (2.2) and substitute the results into the equivalent ignition condition $\tilde{h} = e$, in which $\tilde{h}$ is given by (2.6). Consequently we can obtain

$$h = \frac{e\lambda_g T_a^2 (1 - T_\infty/T_s)^2}{2\gamma R_0^2 T_s^2} \left(\frac{\mathrm{d}\theta}{\mathrm{d}\tilde{r}}\right)^2_{\tilde{r}=1}, \tag{2.12}$$

where $\gamma = c_{pg}/c_{vg}$ is the heat capacity ratio. With knowledge of h given by (2.12), the non-dimensional effective heat loss coefficient can be determined according to (2.6) as

$$\tilde{h}(T_s) = \frac{\alpha_g T_a (1 - T_\infty/T_s)^2 \exp(T_a/T_s + 1)}{2BR_0^2 (T_{ad} - T_\infty)} \left(\frac{\mathrm{d}\theta}{\mathrm{d}\tilde{r}}\right)^2_{\tilde{r}=1}, \tag{2.13}$$

where $\alpha_g = \lambda_g/\rho_g c_{pg}$ is the thermal diffusivity of the combustible mixture. Equation (2.13) indicates that the effective heat loss coefficient is inversely proportional to the surface area of the particle, i.e. $\tilde{h} \sim 1/R_0^2$. This means that ignition becomes more difficult for smaller particles, which is consistent with previous experimental and numerical results. In addition, (2.13) demonstrates that the effective heat loss coefficient varies with the square of the normalized temperature gradient on the particle surface, which substantially increases in the presence of convective heat transfer. Therefore, the relative motion between the hot particle and the combustible mixture may greatly affect the ignition behaviour.

Taking the derivative of $\tilde{h}$ with respect to T_s, one obtains

$$\frac{\mathrm{d}\tilde{h}}{\mathrm{d}T_s} = -\frac{\alpha_g}{2BR_0^2}\left(1 - \frac{T_\infty}{T_s}\right)\left[1 - \frac{T_\infty}{T_s}\left(1 + 2\frac{T_s}{T_a}\right)\right]\frac{T_a^2 e^{T_a/T_s+1}}{T_s^2(T_{ad} - T_\infty)}\left(\frac{\mathrm{d}\theta}{\mathrm{d}\tilde{r}}\right)^2_{\tilde{r}=1}. \tag{2.14}$$

The conditions $T_s \gg T_\infty$ and $T_s/T_a \ll 1$ suggest that $\mathrm{d}\tilde{h}/\mathrm{d}T_s < 0$. Therefore, as the particle temperature falls, the heat loss coefficient becomes larger and thereby heat loss is more pronounced.

The critical ignition temperature, denoted by $T_{ig,cr}$, can be determined by setting $T_s = T_{ig,cr}$ in (2.13) and using the ignition condition of $\tilde{h} = e$. After rearrangement, we have the

following expression the for the critical ignition temperature:

$$\frac{T_a}{T_{ig,cr}} = \ln \frac{2BR_0^2(T_{ad} - T_\infty)}{\alpha_g T_a (1 - T_\infty/T_{ig,cr})^2 (\mathrm{d}\theta/\mathrm{d}\tilde{r})^2_{\tilde{r}=1}}. \tag{2.15}$$

When the particle temperature is greater than the critical ignition temperature, i.e. $T_s > T_{ig,cr}$, the ignition delay time can be evaluated by integrating equation (2.10)

$$\tau_{ig} = \tau_{ch} \int_0^\infty \frac{\mathrm{d}\chi}{e^\chi - \tilde{h}(T_s)\chi}. \tag{2.16}$$

In particular, (2.13) indicates that $\tilde{h}$ vanishes for $(\mathrm{d}\theta/\mathrm{d}\tilde{r})_{\tilde{r}=1} = 0$, i.e. the particle temperature is equal to that in the ambient. In such circumstances, the integral in (2.16) is equal to unity, indicating that $\tau_{ig} = \tau_{ch}$, i.e. ignition occurs under adiabatic conditions. For finite temperature difference, the magnitude of $(\mathrm{d}\theta/\mathrm{d}\tilde{r})_{\tilde{r}=1}$ describes the temperature inhomogeneity. For a spherical particle in a quiescent mixture, the heat transfer is only through thermal conduction and we have $(\mathrm{d}\theta/\mathrm{d}\tilde{r})_{\tilde{r}=1} = -1$, which will be shown in § 3.1. When there is relative motion between the particle and the environment, the heat transfer consists of convection and conduction and we have $|(\mathrm{d}\theta/\mathrm{d}\tilde{r})_{\tilde{r}=1}| > 1$, which will be discussed in §§ 3.2–3.4.

3. The effect of temperature inhomogeneity on ignition by a hot particle

According to (2.13), the temperature gradient on the particle surface, $(\mathrm{d}\theta/\mathrm{d}\tilde{r})_{\tilde{r}=1}$, needs to be obtained so that the effective volumetric heat loss coefficient $\tilde{h}$ can be evaluated, and subsequently the critical ignition temperature can be determined via (2.15). We consider a hot particle placed in a combustible mixture with different flow velocities, including the quiescent situation, creeping flow and flow with separation. For each flow condition, solving the thermal energy equation for the gas mixture yields the temperature distributions, by means of which the temperature gradient on the particle surface $(\mathrm{d}\theta/\mathrm{d}\tilde{r})_{\tilde{r}=1}$ can be evaluated. Adopting two assumptions, that the particle temperature remains constant during the ignition process and that the IFP is anchored at the particle surface, the ignition criterion of the combustible mixture by the hot particle can be described by the critical ignition condition in steady state theory, i.e. $\tilde{h} = e$, which gives the correlation between the critical ignition temperature and various parameters that affect it, e.g. the radius of the particle, the temperature inhomogeneity and the transport properties of the combustible mixture. The fall of the particle temperature and the motion of the IFP lead to transient effects in the ignition process, and their impacts will be discussed in §§ 4 and 5, respectively.

3.1. *Quiescent combustible mixture*

First, we consider the hot particle placed in a quiescent combustible mixture so that the heat transfer at the surface is pure conduction. So far, we have assumed that the particle temperature is constant during the ignition process. The solution of the thermal equation for a solid particle presented in § 4 will confirm that the effect of particle cooling is negligible before ignition occurs. For a particle with a constant temperature, we can employ the quasi-steady state assumption to deal with heat transfer at the particle surface.

The energy equation for the gas mixture can be written in the form (Leal 2007)

$$\tilde{\nabla}^2\theta = 0, \tag{3.1}$$

where $\tilde{\nabla} = R_0\nabla$ is the non-dimensional gradient operator. The solution of (3.1) satisfying the boundary conditions of $\theta = 1$ at $\tilde{r} = 1$ and $\theta = 0$ as $r \to \infty$ is

$$\theta = \frac{1}{\tilde{r}}. \tag{3.2}$$

Accordingly, the non-dimensional temperature gradient on the particle surface is

$$-\left(\frac{\mathrm{d}\theta}{\mathrm{d}\tilde{r}}\right)_{\tilde{r}=1} = 1. \tag{3.3}$$

3.2. *Creeping flow without separation for* $\boldsymbol{Re} \ll 1$

In the presence of relative motion between the particle and the ambient gas, convection contributes to additional heat transfer, and the energy equation should be revised to

$$Pe(\tilde{\boldsymbol{u}} \cdot \tilde{\nabla}\theta) = \tilde{\nabla}^2\theta, \tag{3.4}$$

where the non-dimensional velocity $\tilde{\boldsymbol{u}}$ is normalized by the uniform flow velocity, U_∞, of the ambient gas, i.e. $\tilde{\boldsymbol{u}} = \boldsymbol{u}/U_\infty$. The Péclet number is defined as $Pe = U_\infty R_0/\alpha_g$. The Péclet number can equivalently be written as the product of the Reynolds number, $Re = U_\infty R_0/\nu_g$, and the Prandtl number, $Pr = \nu_g/\alpha_g$, where ν_g is the kinematic viscosity of the ambient gas. The Prandtl number depends only on the fluid properties and is around unity for most gases under atmospheric pressure at room temperature. Consequently, the Péclet number and the Reynolds number are of the same order, i.e. $Pe \sim Re$.

The flow field is affected by changing the Reynolds number. For creeping flow with $Re \ll 1$, i.e. the flow velocity distribution can be described by the Stokes solution (Landau & Lifshitz 1987)

$$\tilde{u}_r = -\cos\phi\left(1 - \frac{3}{2\tilde{r}} + \frac{1}{2\tilde{r}^3}\right), \quad \tilde{u}_\phi = -\sin\phi\left(1 - \frac{3}{4\tilde{r}} - \frac{1}{4\tilde{r}^3}\right), \tag{3.5a,b}$$

where ϕ represents the polar angle and its origin ($\phi = 0$) is selected at the front stagnation point of the sphere, and thereby $\phi = \pi$ corresponds to the rear stagnation point.

For $Re \ll 1$ and $Pe \sim Re$, the temperature distribution can be expanded in asymptotic series in terms of Pe. However, separate solutions must be sought respectively in the inner region for $1 \le \tilde{r} \le O(Pe^{-1})$, where the heat conduction term is much larger than the convection term, and in the outer region for $O(Pe^{-1}) < \tilde{r} < \infty$, where the convection term is of equal importance to the conduction term. The detailed derivation of the asymptotic solution of the temperature distribution can be found in Leal (2007), and here we only briefly present key processes.

In the inner region, the proper length scale is R_0, and the asymptotic series for θ in terms of Pe is

$$\theta_{in} = \theta_{in,0}(\tilde{r}, \phi) + Pe\theta_{in,1}(\tilde{r}, \phi) + O(Pe^2). \tag{3.6}$$

Substituting equation (3.6) into (3.4) and collecting terms of like powers of Pe, one obtains the leading-order solution $\theta_{in,0} = 1/\tilde{r}$, and the first-order correction $\theta_{in,1}$ which

satisfies the following equation

$$\tilde{\nabla}^2\theta_{in,1} = \tilde{\boldsymbol{u}} \cdot \nabla\theta_{in,0}. \tag{3.7}$$

The solution of (3.7) subject to the boundary condition of $\theta_{in,1} = 0$ at $\tilde{r} = 1$ can be written as

$$\theta_{in,1} = \sum_{n=0}^{\infty} A_n[\tilde{r}^n - \tilde{r}^{-(n+1)}]P_n(-\eta) + \left(\frac{1}{2} - \frac{3}{4\tilde{r}} + \frac{3}{8\tilde{r}^2} - \frac{1}{8\tilde{r}^3}\right)P_1(-\eta), \tag{3.8}$$

where P_n represents the Legendre polynomial of order n, and $\eta = \cos\phi$. The integration constants A_n should be determined through matching with the asymptotic solution in the outer region. The fact that $P_1(-\eta)/2$ does not vanish as $\tilde{r} \to \infty$ suggests that $\theta_{in,1}$ does not satisfy the boundary condition at infinity. Therefore, the solution in the outer region needs to be obtained.

In the outer region, the length scale should be redefined because the temperature distribution appears to be less sensitive to the particle radius at remote distance. A suitable rescaling is $\xi = \tilde{r}Pe$, in terms of which, the leading order of the normalized temperature in the outer region, θ_{out}, satisfies

$$\tilde{\nabla}_{\xi}^2\theta_{out} = -\left[\frac{\partial\theta_{out}}{\partial\xi} + \left(\frac{1-\eta^2}{\xi}\right)\frac{\partial\theta_{out}}{\partial\eta}\right]. \tag{3.9}$$

The right-hand side of the above equation represents the modification of the temperature distribution in the outer region by uniform flow of ambient gas. The solution of (3.9) subject to the boundary condition of $\theta_{out} \to 0$ as $\xi \to \infty$ is

$$\theta_{out} = \sqrt{\frac{\pi}{\chi}}e^{-\chi\eta/2}\sum_{k=0}^{\infty} B_k K_{k+1/2}\left(\frac{\chi}{2}\right)P_k(-\eta), \tag{3.10}$$

where the coefficients B_k must be determined by matching with the inner solution θ_{in}. The functions $K_{k+1/2}$ represent the modified Bessel functions of order $k + 1/2$. The matching of θ_{in} and θ_{out} is conducted in an overlap region in which, $\tilde{r}$ and ξ could be interchangeably selected as the characteristic length scale. From the matching we have

$$A_0 = -\tfrac{1}{2}, \quad A_k = 0 \quad \text{for } k \geq 1, \tag{3.11}$$

$$B_0 = \frac{1}{\pi}, \quad B_k = 0 \quad \text{for } k \geq 1. \tag{3.12}$$

Substituting equations (3.11) and (3.12) into (3.8) and (3.10) respectively, the inner and outer solutions for the normalized temperature are fully determined. The composite solution valid in the whole domain can be constituted by summarizing θ_{in} and θ_{out} and subtracting their common part in the overlapping region, and it is

$$\theta = \frac{1}{\tilde{r}}e^{-\tilde{r}Pe(1+\eta)/2} + Pe\left[\frac{1}{2\tilde{r}} - \eta\left(-\frac{3}{4\tilde{r}} + \frac{3}{8\tilde{r}^2} - \frac{1}{8\tilde{r}^3}\right)\right]. \tag{3.13}$$

In contrast to θ_{in}, the composite solution of θ given by (3.13) satisfies the boundary condition $\theta \to 0$ as $\tilde{r} \to \infty$ at finite Pe. Subsequently, the negative of the temperature

gradient on the particle surface can be obtained as

$$-\left(\frac{\partial\theta}{\partial\tilde{r}}\right)_{\tilde{r}=1}=\frac{1}{2}\left(1+\frac{3}{4}\eta\right)Pe+e^{-(1+\eta)Pe/2}\left[1+\frac{1}{2}(1+\eta)Pe\right]. \tag{3.14}$$

The heat transfer rate changes with polar angle, represented by $\eta=\cos\phi$. It takes the largest and smallest values at the front ($\eta=1$) and rear ($\eta=-1$) stagnation points, respectively, i.e.

$$-\left(\frac{\partial\theta}{\partial\tilde{r}}\right)_{\tilde{r}=1,max}=e^{-Pe}(1+Pe)+\frac{7}{8}Pe\approx 1+\frac{7}{8}Pe, \tag{3.15}$$

$$-\left(\frac{\partial\theta}{\partial\tilde{r}}\right)_{\tilde{r}=1,min}=1+\frac{1}{8}Pe. \tag{3.16}$$

The heat transfer on the particle surface plays the role of heat loss during the ignition process. Equations (3.15) and (3.16) indicate that ignition first occurs at the rear stagnation point (i.e. $\phi=\pi$) where the temperature inhomogeneity is the smallest over the particle surface. This is consistent with previous simulation results (Zirwes *et al.* 2019; Wang *et al.* 2021).

3.3. *Boundary layer flow with separation for* $\boldsymbol{Re}\gg 1$

At high Reynolds number, i.e. increasing either the particle size or the flow velocity of the ambient gas, flow separation takes place at the rear hemisphere of the spherical particle. The IFP adjacent to the particle surface continues to absorb thermal energy from the front stagnation location to the separation point, beyond which the IFP is taken away from the particle surface by the recirculating flow. The relative motion between the particle and the combustible mixture facilitates the heat transfer on the particle surface due to convection, which thereby increases the critical ignition temperature.

Previous studies (Mével *et al.* 2016, 2019; Melguizo-Gavilanes *et al.* 2017*a*,*b*) demonstrated that, at the critical ignition state, i.e. $T_s=T_{cr}$, ignition first occurs around the separation point. This can be understood as follows. Flow decelerates on approaching the separation point, suggesting that convective heat transfer becomes less intensive and hence decreases the heat loss for ignition. Near the separation point, the temperature variation becomes gentle and thereby provides favourable conditions for ignition. Accordingly, we define the critical ignition condition based on the assumption that the resulting ignition location coincides with the separation point, where the local temperature gradient has the least magnitude and thus preferentially supports ignition. Moreover, the IFP would be taken away from the hot particle passing over the separation point and therefore lose the capability of ignition. While, as the particle temperature continues to increase, the ignition location moves upstream since an elevation of particle temperature can sustain more severe heat loss during ignition.

For large Reynolds number, i.e. $Re\gg 1$, the flow field consists of a boundary layer on the particle surface. Across the boundary layer, the flow velocity decelerates to zero on the particle surface. In the outer region above the boundary layer, viscous stress can be neglected. For uniform flow across a spherical particle, the velocity components in the

outer region are given by (Leal 2007; Schlichting & Gersten 2016)

$$\tilde{u}_\phi = \left(1 + \frac{1}{2\tilde{r}^3}\right)\sin\phi, \quad \tilde{u}_r = -\left(1 - \frac{1}{\tilde{r}^3}\right)\cos\phi. \tag{3.17a,b}$$

On the particle surface with $\tilde{r} = 1$, the radial component becomes zero while the tangential component is $\tilde{u}_{\phi,\tilde{r}=1} = (3/2)\sin\phi \neq 0$, which does not satisfy the no-slip condition. This indicates the necessity of solving the velocity distribution in the momentum boundary layer.

The boundary layer theory suggests rescaling the non-dimensional transverse coordinate and velocity component, defined by

$$Y = \sqrt{Re}(\tilde{r} - 1), \quad V = \tilde{u}_r\sqrt{Re}, \tag{3.18a,b}$$

for suitable description of the velocity distribution in the boundary layer. In the limit of $Re \to \infty$, the governing equations for the momentum boundary layer covering a spherical particle are

$$\frac{\partial V}{\partial Y} + \frac{1}{\sin\phi}\frac{\partial}{\partial\phi}(u\sin\phi) = 0, \tag{3.19}$$

$$\frac{\partial^2 u}{\partial Y^2} = \frac{\mathrm{d}p}{\mathrm{d}\phi} + V\frac{\partial u}{\partial Y} + u\frac{\partial u}{\partial\phi}, \tag{3.20}$$

where we denote the non-dimensional tangential component of the flow velocity in the momentum boundary layer by u. Since the flow outside the momentum boundary layer is almost potential, the pressure gradient can be solved in terms of the $\tilde{u}_\phi$ given by (3.17*a*,*b*) based on Bernoulli's equation, which, at the particle surface $\tilde{r} = 1$, yields

$$\frac{\mathrm{d}p}{\mathrm{d}\phi} = -\tilde{u}_{\phi,\tilde{r}=1}\frac{\mathrm{d}\tilde{u}_{\phi,\tilde{r}=1}}{\mathrm{d}\phi} = -\frac{9}{8}\sin 2\phi, \tag{3.21}$$

where the pressure is non-dimensionalized by $\rho_g U_\infty^2$.

Equations (3.19) and (3.20) can be solved by means of a Blasius series, i.e. a series of velocity components in terms of ϕ^n with n being integer. The detailed description of the mathematical method can found in Leal (2007) and Schlichting & Gersten (2016). Here, we only briefly present key steps in our solution.

According to (3.17*a*,*b*), the tangential component of the potential flow $\tilde{u}_\phi$ at $\tilde{r} = 1$ can be expanded in a series of ϕ,

$$\tilde{u}_{\phi,\tilde{r}=1} = \tfrac{3}{2}\sin\phi = \tfrac{3}{2}\phi - \tfrac{1}{4}\phi^3 + \tfrac{1}{80}\phi^5 - \tfrac{1}{3360}\phi^7 + \cdots. \tag{3.22}$$

Correspondingly, the tangential velocity in the momentum boundary layer can also be expanded as a series of ϕ with coefficients being general functions of the rescaled transverse coordinate Y. To obtain a relatively accurate interpretation to the velocity profile in the rear hemisphere, we retain terms of ϕ^n with $n \leq 7$ in the expansion of u, i.e.

$$u = F_1'(Y)\phi + F_3'(Y)\phi^3 + F_5'(Y)\phi^5 + F_7'(Y)\phi^7, \tag{3.23}$$

where the prime in coefficient function F refers to derivative with respect to Y. The no-slip boundary condition requires that the coefficient functions F's satisfy

$$F_1'(0) = F_3'(0) = F_5'(0) = F_7'(0) = 0. \tag{3.24}$$

Matching with outer potential flow suggests that

$$F_1'(Y) \to \tfrac{3}{2}, \quad F_3'(Y) \to -\tfrac{1}{4}, \quad F_5'(Y) \to \tfrac{1}{80}, \quad F_7'(Y) \to -\tfrac{1}{3360} \text{ as } Y \to \infty. \tag{3.25}$$

Substituting the series of u given by (3.23) into the continuity equation (3.19), one obtains the series for $\partial V/\partial Y$. Integrating with respect to Y yields

$$\begin{aligned} V = &-2F_1 + (\tfrac{1}{3}F_1 - 4F_3)\phi^2 + (\tfrac{1}{45}F_1 + \tfrac{1}{3}F_3 - 6F_5)\phi^4 \\ &+ (\tfrac{2}{945}F_1 + \tfrac{1}{45}F_3 + \tfrac{1}{3}F_5 - 8F_7)\phi^6, \end{aligned} \tag{3.26}$$

whose coefficients are functions of F_i values instead of their derivative with respect to Y. The no-penetration boundary condition on the particle surface, i.e. $V = 0$ at $Y = 0$, requires that the functions F satisfy

$$F_1(0) = F_3(0) = F_5(0) = F_7(0) = 0. \tag{3.27}$$

Substituting the series forms of (3.23) and (3.26) into the momentum equation (3.20) and collecting the powers of ϕ, we have

$$F_1''' + 2F_1F_1'' - F_1'^2 + \tfrac{9}{4} = 0, \tag{3.28}$$

$$F_3''' + 2F_1F_3'' - 4F_1'F_3' - F_1''(\tfrac{1}{3}F_1 - 4F_3) - \tfrac{3}{2} = 0, \tag{3.29}$$

$$\begin{aligned} &F_5''' + 2F_1F_5'' - 6F_1'F_5' - \tfrac{1}{45}F_1''(F_1 + 15F_3 - 270F_5) \\ &-F_3''(\tfrac{1}{3}F_1 - 4F_3) - 3F_3'^2 + \tfrac{3}{10} = 0, \end{aligned} \tag{3.30}$$

$$\begin{aligned} &F_7''' + 2F_1F_7'' - 8F_1'F_7' - \tfrac{1}{945}F_1''(2F_1 + 21F_3 + 315F_4 - 7560F_7) \\ &-F_5''(\tfrac{1}{3}F_1 - 4F_3) - 8F_3'F_5' - \tfrac{1}{45}F_3''(F_1 + 15F_3 - 270F_5) - \tfrac{1}{35} = 0, \end{aligned} \tag{3.31}$$

Which, subject to boundary conditions given by (3.24), (3.25) and (3.27), and can be solved numerically.

With knowledge of F_i values, the profiles of u and V can be determined through (3.23) and (3.26), respectively. According to the boundary layer theory, the separation point is characterized by the relation (Leal 2007)

$$\left(\frac{\partial u}{\partial Y}\right)_{Y=0,\phi=\phi_{sep}} = 0, \tag{3.32}$$

which, with our numerical results of u and V, gives $\phi_{sep} \approx 108^\circ$ and is consistent with previous studies (Schlichting & Gersten 2016). This separation angle holds for $Re \to \infty$ which can be understood as meaning that the boundary layer equations (3.19) and (3.20) in fact give the leading-order solution of the flow field at the limit $Re \to \infty$. For moderate Re, the polar angle representing the separation point moves downstream on reducing the Reynolds number (Rimon & Cheng 1969). To interpret such relation, we have to retain higher-order terms in the boundary layer equations, which results in exceeding difficulty in the mathematics and is thus beyond the scope of the present study.

Figure 1 shows that the tangential velocity increases from zero on the particle surface to the potential flow solution in the outer region. According to (3.21), the outer potential flow accelerates from the front stagnation point ($\phi = 0$) to the peripheral side of the sphere ($\phi = \pi/2$), after which the pressure gradient becomes adverse, leading to flow separation around $\phi \approx 0.6\pi = 108^\circ$.

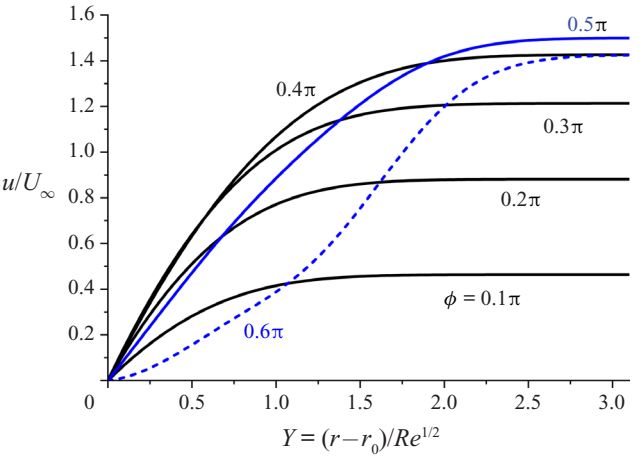

Figure 1. Change of the tangential velocity u with scaled transverse coordinate Y across the momentum boundary layer for different polar angles of $\phi = 0.1\pi \sim 0.6\pi$.

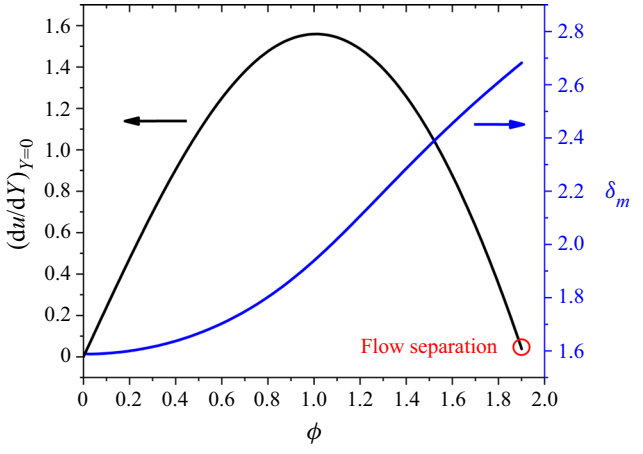

Figure 2. Change of the tangential velocity gradient adjacent to the particle surface and the thickness of the momentum boundary layer with polar angle ϕ.

The outer edge of the boundary layer is characterized by $u = 0.99\tilde{u}_{\phi,\tilde{r}=1}$, and its distance from the particle surface is defined as the thickness of the momentum boundary layer, denoted by δ_m. Figure 2 shows that δ_m increases monotonically with ϕ, particularly beyond $\phi = \pi/4$, where the favourable pressure gradient at $Y = 0$ is of largest magnitude according to (3.21). Besides, the tangential velocity gradient, interpreting the frictional resistance experienced by the particle, achieves the largest value around $\phi = 1.0$ and vanishes around $\phi_{sep} = 0.6\pi$. This is consistent with the velocity profiles shown in figure 1.

Since $Pe \sim Re$, large Reynolds number also implies that $Pe \gg 1$. This indicates that the temperature of the gaseous premixture also exhibits a rapid transition from $\theta = 1$ on the particle surface to $\theta \to 0$ in the ambient, which is known as the thermal boundary layer. Since the Prandtl number of the gaseous premixture is of $O(1)$, the rescaling relation (3.18*a*,*b*) holds in the thermal boundary layer as well. Therefore, neglecting dissipation of

kinetic energy to thermal energy, the governing equation for the thermal boundary layer can be written in the following form:

$$u\frac{\partial\theta}{\partial\phi}+V\frac{\partial\theta}{\partial Y}=\frac{1}{Pr}\frac{\partial^2\theta}{\partial Y^2}, \tag{3.33}$$

where the coefficients u and V, given by (3.23) and (3.26), are known functions of ϕ and Y. Equation (3.33) is subject to the following boundary conditions:

$$\theta=1 \text{ at } Y=0, \tag{3.34}$$

$$\theta\to 0 \text{ as } Y\to\infty. \tag{3.35}$$

In analogy to the Blasius series representing the velocity profiles u and V, the normalized temperature in the thermal boundary layer can also be expanded in the series form as

$$\theta=H_0(Y)+H_2(Y)\phi^2+H_4(Y)\phi^4+H_6(Y)\phi^6. \tag{3.36}$$

Since the temperature profile is an even function about the axis of symmetry, i.e. $\theta(\phi)=\theta(-\phi)$, only terms of even power in ϕ appear. To obtain consistent accuracy with the Blasius series of the velocity profiles, we retain four terms up to ϕ^6. Substituting the series representations of u, V and θ, given by (3.23), (3.36) and (3.36), respectively, into (3.33), we obtain

$$\frac{H_0''}{Pr}=-2F_1H_0', \tag{3.37}$$

$$\frac{H_2''}{Pr}=\left(\frac{F_1}{3}-4F_3\right)H_0'+2F_1'H_2-2F_1H_2', \tag{3.38}$$

$$\frac{H_4''}{Pr}=\left(\frac{F_1}{45}+\frac{F_3}{3}-6F_5\right)H_0'+2F_3'H_2+\left(\frac{F_1}{3}-4F_3\right)H_2'+4F_1'H_4-2F_1H_4', \tag{3.39}$$

$$\begin{aligned}\frac{H_6''}{Pr}=&\left(\frac{2F_1}{945}+\frac{F_3}{45}+\frac{F_5}{3}-8F_7\right)H_0'+2F_5'H_2+\left(\frac{F_1}{45}+\frac{F_3}{3}-6F_5\right)H_2'+4F_3'H_4\\&+\left(\frac{F_1}{3}-4F_3\right)H_4'+6F_1'H_6-2F_1H_6'.\end{aligned} \tag{3.40}$$

The boundary conditions for H_i are given by

$$H_0(0)=1,\quad H_2(0)=H_4(0)=H_6(0)=0, \tag{3.41}$$

$$H_0(Y)=H_2(Y)=H_4(Y)=H_6(Y)=0 \text{ as } Y\to\infty. \tag{3.42}$$

The numerical solution to (3.37)–(3.40) subject to boundary conditions (3.41) and (3.42) can be sought following the same procedure as that used to obtain the coefficients F_i for the Blasius series of u and V. The representative parameter of the Prandtl number is selected to be that of air, i.e. $Pr=0.71$, in the numerical solution.

Figure 3 indicates that the normalized temperature tends to decrease linearly with Y around the particle surface, whose slope continues to reduce as ϕ increases. At some elevated distance in the transverse direction, the change of θ becomes very slow and exhibits a long tail on relaxing to $\theta=0$. The outer edge of the thermal boundary layer

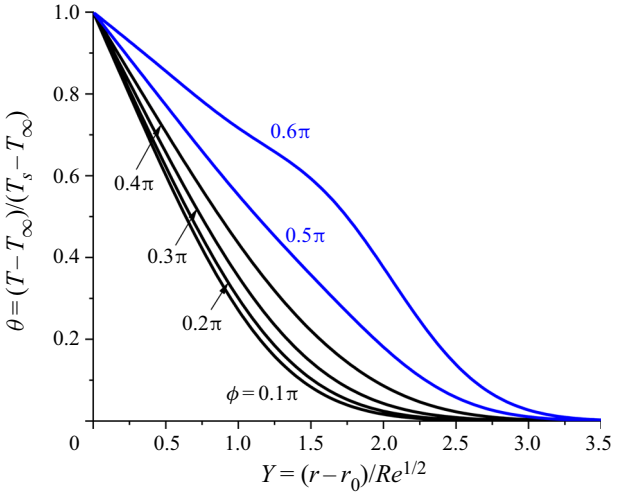

Figure 3. Change of the normalized temperature with scaled transverse coordinate across the thermal boundary layer for different polar angles of $\phi = 0.1\pi \sim 0.6\pi$.

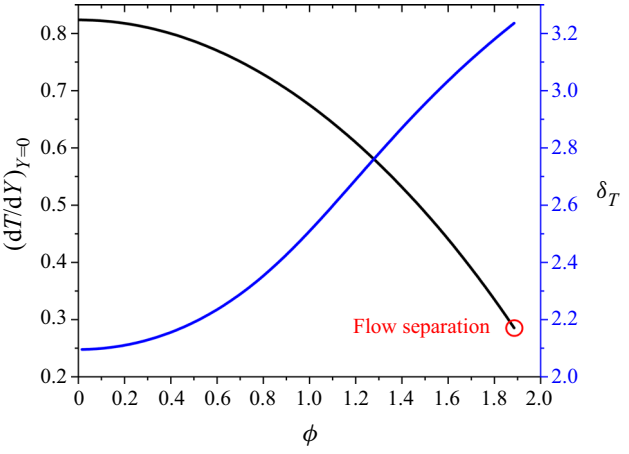

Figure 4. Change of the temperature gradient adjacent to the particle surface and the thickness of the thermal boundary layer with polar angle ϕ.

refers to the transverse coordinate where $\theta = 0.01$, and its distance from the particle surface is defined as the thickness of the thermal boundary layer, denoted by δ_T.

Figure 4 shows the temperature gradient adjacent to the particle surface and the thickness of the thermal boundary layer. Similar to δ_m, the thermal boundary layer grows monotonically with ϕ. Besides, comparison between figures 2 and 4 indicates that the thermal boundary layer is thicker than the momentum boundary layer. This is because $Pr < 1$.

The rate of heat transfer on the particle surface can be quantified by the magnitude of the temperature gradient there, which, as seen from figure 4, decreases to almost one third from the front stagnation point to the separation point. According to (2.13), the fall in temperature gradient reduces the heat loss for ignition of the combustible mixture. This is consistent with the experimental observation (Coronel 2016; Coronel *et al.* 2018)

that ignition most probably takes place near the separation point, where the temperature gradient calculated from (3.36) is

$$-\left(\frac{\partial\theta}{\partial\tilde{r}}\right)_{\tilde{r}=1,\phi=\phi_{sep}} = \sqrt{Re}[H_0'(0) + H_2'(0)\phi_{sep}^2 + H_4'(0)\phi_{sep}^4 + H_6'(0)\phi_{sep}^6] = 0.276\sqrt{Re}. \tag{3.43}$$

3.4. *The critical ignition temperature*

According to (2.13), the non-dimensional heat loss coefficient is proportional to the square of the temperature gradient. Consequently, ignition occurs at the point where the magnitude of the local temperature gradient is the smallest, which is defined as the ignition temperature gradient, denoted by $(\mathrm{d}\theta/\mathrm{d}\tilde{r})_{ig}$. In a quiescent environment, the temperature gradient is uniform over the particle surface according to (3.3), yielding

$$-(\mathrm{d}\theta/\mathrm{d}\tilde{r})_{ig,0} = 1. \tag{3.44}$$

For creeping flow over the hot particle, the lowest heat transfer rate occurs at the rear stagnation point, for which the temperature gradient is given by (3.16). Consequently, the ignition temperature gradient for creeping flow is

$$-(\mathrm{d}\theta/\mathrm{d}\tilde{r})_{ig,c} = 1 + \tfrac{1}{8}RePr. \tag{3.45}$$

At large Re, flow separation takes place and the ignition temperature can be evaluated by the boundary layer solution given by (3.43). Therefore, the ignition temperature gradient for large Re is

$$-(\mathrm{d}\theta/\mathrm{d}\tilde{r})_{ig,\infty} = 0.276\sqrt{Re}. \tag{3.46}$$

The correlations between the ignition temperature gradients and the Reynolds number for $Re \ll 1$ and $Re \to 1$ are respectively presented by (3.45) and (3.46). However, for hot particle induced ignition, the Reynolds number usually varies in the intermediate range from $O(1)$ to $O(10^2)$, in which there exists a gap in the ignition temperature gradients predicted by (3.45) and (3.46) because the controlling mechanism of heat transfer alters as Re increases.

Since the Blasius series holds at the limit condition of $Re \to \infty$, the result given by (3.46) is not qualitatively accurate in the intermediate range of Re. It would be convenient to obtain an explicit formula that can predict the ignition temperature gradient in a wide range of Reynolds numbers from $Re = 0$ (for pure conduction) to $Re \sim O(10^2)$ (flow separation without unsteady vortex shedding) (Johnson & Patel 1999; Schlichting & Gersten 2016). Combining the mathematical forms of (3.45) and (3.46), we can specify the dependence of $(\mathrm{d}\theta/\mathrm{d}\tilde{r})_{ig}$ on Re in the following form:

$$-(\mathrm{d}\theta/\mathrm{d}\tilde{r})_{ig,m} = 1 + \alpha_T Re^{1/2}, \tag{3.47}$$

which reduces to pure conduction for $Re = 0$ and scales with $\sqrt{Re}$ for large Reynolds numbers. The parameter α_T shall be determined with the help of the Frossling formula (Hughmark 1980; McAllister, Chen & Fernandez-Pello 2011). The detailed procedures are presented as follows.

The Frossling formula (Hughmark 1980; McAllister *et al.* 2011) interprets the total heat transfer from the particle in terms of the Nusselt number, which can be equivalently

correlated to an average temperature gradient, i.e.

$$-(\mathrm{d}\theta/\mathrm{d}\tilde{r})_{av,m} = 1 + 0.282Re^{1/2}Pr^{1/3}. \tag{3.48}$$

In spite of a similar mathematical form, the coefficient α_T in (3.47) differs from that in (3.48). Considering similarity in the boundary layer, we suppose that the proportionality between the temperature gradient at the flow separation point, $(\mathrm{d}\theta/\mathrm{d}r)_{ig,m}$ given by (3.47), and its average value over the whole particle surface, $(\mathrm{d}\theta/\mathrm{d}r)_{ave}$ given by (3.48), would be less than unity and tends to vary slowly with Re. Thereby, we can determine the coefficient α_T with the help of both the Frossling formula and the Blasius series solution of thermal boundary layer.

The average temperature gradient in the limit of $Re \to \infty$ can be calculated via the boundary layer solution, giving

$$-(\mathrm{d}\theta/\mathrm{d}\tilde{r})_{av,\infty} = -\left(\int_0^{\phi_{sep}} \sin\phi\,\mathrm{d}\phi\right)^{-1} \int_0^{\phi_{sep}} (\mathrm{d}\theta/\mathrm{d}\tilde{r})_{\tilde{r}=1} \sin\phi\,\mathrm{d}\phi = 0.582\sqrt{Re}, \tag{3.49}$$

where $\phi_{sep} \approx 108^\circ$ as obtained before and (3.36) is used.

Therefore, the ratio in the limit of $Re \to \infty$ can be determined,

$$c_\infty = \frac{(\mathrm{d}\theta/\mathrm{d}\tilde{r})_{ig,\infty}}{(\mathrm{d}\theta/\mathrm{d}\tilde{r})_{av,\infty}} = 0.474. \tag{3.50}$$

If we assume that the value of c_∞ is independent of the Reynolds number, then we can determine the parameter α_T in the limit of $Re \to \infty$ through the subsequent relation,

$$\lim_{Re\to\infty} \frac{(\mathrm{d}\theta/\mathrm{d}\tilde{r})_{ig,m}}{(\mathrm{d}\theta/\mathrm{d}\tilde{r})_{av,m}} = \frac{\alpha_T}{0.282Pr^{1/3}} \to 0.474, \tag{3.51}$$

which gives $\alpha_T = 0.117$ for $Pr = 0.71$. Substituting the value of α_T into (3.47), the ignition temperature gradient in this intermediate range of Re can be determined.

Substituting equation (3.47) into (2.13), we obtain the effective heat loss coefficient in the presence of relative motion between hot particle and the combustible mixture

$$\tilde{h}(T_s) = \frac{\alpha_g T_a (1 - T_\infty/T_s)^2 e^{T_a/T_s+1}}{2BR_0^2 T_{ad}(1 - T_\infty/T_{ad})}(1 + \alpha_T Re^{1/2})^2. \tag{3.52}$$

This expression indicates that the non-dimensional heat loss coefficient increases monotonically with the Reynolds number. The critical ignition temperature $T_{ig,cr}$ can be determined by substituting equation (3.47) into (2.15), which gives

$$\frac{T_a}{T_{ig,cr}} = \ln \frac{2T_{ad}(1 - T_\infty/T_{ad})R_0^2 B}{T_a(1 - T_\infty/T_{ig,cr})^2 \alpha_g} - 2\ln(1 + \alpha_T Re^{1/2}). \tag{3.53}$$

In quiescent environment with $Re = 0$, the second term on the right-hand side of (3.53) vanishes and we have

$$\frac{T_a}{T_{ig,cr}} = \ln \frac{2T_{ad}(1 - T_\infty/T_{ad})R_0^2 B}{T_a(1 - T_\infty/T_{ig,cr})^2 \alpha_g}, \tag{3.54}$$

which is equivalent to the ignition theory given by the steady state theory with $\Delta_I = 1$. In the absence of relative motion between the particle and the combustible mixture, the

temperature inhomogeneity is attributed solely to heat conduction at the particle surface, and thus depends on the square of the particle radius.

Usually, $T_{ig,cr}$ and T_{ad} are much higher than T_∞, and thereby we can assume $1 - T_\infty/T_{ig,cr} \approx 1$ and $1 - T_\infty/T_{ad} \approx 1$. Accordingly, a simplified ignition criterion can be obtained from (3.54)

$$\frac{T_a}{T_{ig,cr}} \approx \ln \frac{2T_{ad}BR_0^2}{T_a\alpha_g}, \tag{3.55}$$

which shows that the inverse of the critical ignition temperature is linearly proportional to the logarithm of the particle radius or the surface area. It agrees with the scaling relation for ignition in a stagnant environment proposed by Laurendeau (1982).

To determine the critical ignition temperature through (3.53), we need to know the reaction rate factor B and activation temperature T_a. In this work, we consider both CH_4/air and H_2/air mixtures in stoichiometric conditions, and accordingly, the parameters B and T_a for an individual mixture should be determined independently by fitting the ignition delay time calculated from simulation using detailed chemistry based on (2.5). According to ignition behaviour, we specify the reaction related parameters for the CH_4/air mixture at a relatively high temperature range, e.g. $T > 1500$ K, giving $B = 9.5 \times 10^8$ s^{-1} and $T_a = 25\,000$ K, and for the H_2/air mixture at a comparably lower temperature range, e.g. $T > 900$ K, obtaining, $B = 10^{14}$ s^{-1} and $T_a = 28\,500$ K.

Figure 5 compares the critical ignition temperature predicted by the present theory, i.e. (3.54), and previous simulations and experiments. Good agreement is shown to be achieved. For both CH_4/air and H_2/air mixtures, the critical ignition temperature $T_{ig,cr}$ is shown to increase rapidly when the particle radius R_0 decreases. In particular, $T_{ig,cr}$ for CH_4/air for is around 1500 K at $R_0 = 1$ mm, while it is around 2200 K at $R_0 = 0.1$ mm. The quantitative difference between theoretical prediction and numerical/experimental results may be primarily attributed to the simplified one-step reaction model considered in present analysis. According to the numerical study by Häber *et al.* (2017), the critical ignition temperature of spherical particle (with radius 0.8 mm) determined using the Gas Research Institute (GRI) 3.0 mechanism tends to be uniformly lower than that calculated utilizing the University of California at San Diego (UCSD) mechanism for a wide range of stoichiometric ratios, and the maximum difference could be greater than 50 K. This suggests that the chemical reaction mechanism has a considerable effect on the quantitative evaluation of the critical ignition temperature.

The actual chemical reaction involves multiple stages and various elementary rate coefficients, which can hardly be characterized by two constant parameters (activation temperature and reaction frequency) in a wide range of temperatures. Generalizing the activation temperature and reaction frequency as functions of temperature, i.e. $T_a = T_a(T)$ and $B = B(T)$, would improve the accuracy of the reaction model, which, however, is beyond the scope of the present study.

In this work, we neglected the effect of thermal radiation from the hot particle to the combustible mixture in the environment. Based on scaling analysis, the rate of heat transfer per unit area due to radiation and conduction can be evaluated as $h_{radiation} \sim \alpha_r\sigma T^4$ and $h_{conduction} \sim \lambda\nabla T$, respectively, where σ is the Stefan–Boltzmann constant, and $\alpha_r < 1$ indicates the deviation from black-body radiation. For particles with of temperature around 1000 K and radius around 1 mm, the magnitudes of $h_{conduction}$ and $h_{radiation}$ approximately satisfy $h_{conduction}/h_{radiation} \sim 1/2\alpha_r$. However, the emissivity α_r in this temperature range would be considerably smaller than unity (corresponding to black-body radiation) and

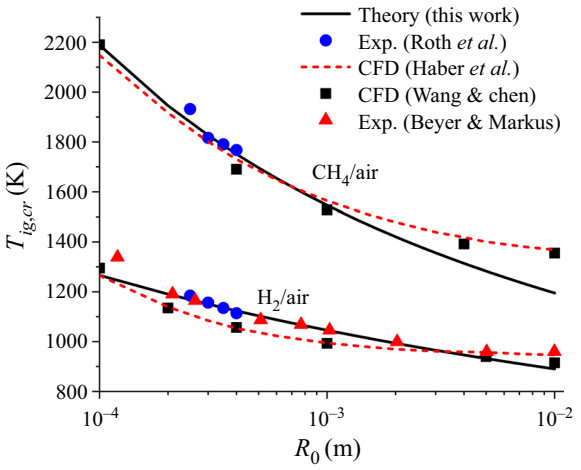

Figure 5. Change of the critical ignition temperature with the particle radius. The mixture is stoichiometric CH_4/air at 300 K and 1 atm. The theoretical results are from (3.54); the experimental data were reported by Roth *et al.* (2017); and the simulation results are from Beyer & Markus (2012), Häber *et al.* (2017) and Wang & Chen (2020).

thus the rate of heat transfer by conduction would be greater than that due to radiation. Besides, the radiative heat transfer is of long range, i.e. only a slight portion of the thermal energy carried by the propagating electromagnetic waves could be absorbed by the reactive mixture close to the particle surface. Therefore, thermal radiation of the hot particle on the ignition of combustible mixture should be secondary.

For particle in non-static mixture, i.e. $Re > 0$, the second term on the right-hand side of (3.53) is greater than zero, suggesting that the enhanced temperature inhomogeneity due to convective heat transfer tends to increase the critical ignition temperature. For small Reynolds number, (3.53) can be simplified to

$$\frac{T_a}{T_{ig,cr}} \approx \ln \frac{2T_{ad}R_0^2 B}{T_a \alpha_g} - 2\alpha_T Re^{1/2}, \tag{3.56}$$

while at large Reynolds number it becomes

$$\frac{T_a}{T_{ig,cr}} \approx \ln \frac{2T_{ad}R_0^2 B}{T_a \alpha_g} - \ln(\alpha_T^2 Re). \tag{3.57}$$

Equations (3.56) and (3.57) show that the relative motion between the particle and the ambient gas increases the critical ignition temperature, and that $T_{ig,cr}$ increases with the Reynolds number. Nevertheless, the logarithmic scaling relation between $T_{ig,cr}$ and U_∞ (proportional to Reynolds number) appears to differ from the fitting formulas given by Zirwes *et al.* (2019), which interpret $T_{ig,cr}$ as power functions of U_∞.

Figure 6 plots the critical ignition temperature predicted by the present analysis and simulations in Zirwes *et al.* (2019). Using the average temperature gradient in (3.48) greatly overestimates the heat loss coefficient and thereby the critical ignition temperature. On the contrary, the ignition temperature gradient given by (3.47) appropriately evaluates the temperature inhomogeneity at the ignition location and thereby has predictions agreeing well with those from simulations. The slight elevation of the theoretically predicted critical ignition temperature can be attributed to the fact that the viscosity of

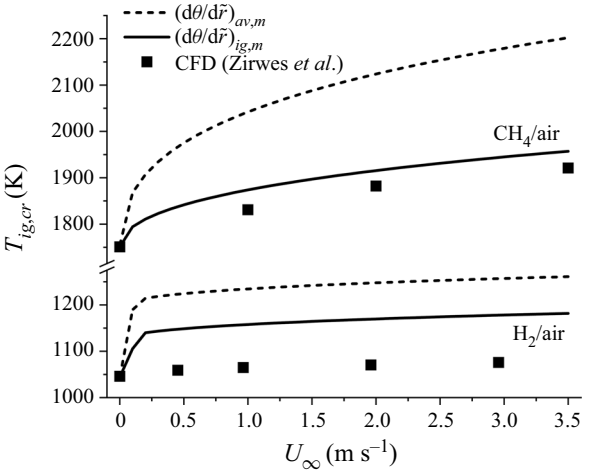

Figure 6. Change of the critical ignition temperature with flow velocity. Stoichiometric mixtures of CH_4/air and H_2/air are considered at conditions of 300 K and 1 atm, and the particle radius is 0.4 mm. The solid line represents prediction by (3.53) in comparison with the dashed line obtained by replacing $(d\theta/d\tilde{r})_{ig,m}$ with $(d\theta/d\tilde{r})_{av,m}$ given by (3.48). The symbols denote simulation results in Zirwes *et al.* (2019).

the gaseous mixture is evaluated based on the far-field temperature rather than the particle temperature, which results in a larger Reynolds number and thereby a greater temperature gradient at the ignition location.

Based on energy budget analysis, Häber *et al.* (2017) proposed a theoretical formula for the ignition temperature, which scales with R_0 in the form of $T_a/T_{ig,cr} \sim \ln(R_0^2/\sqrt{Re})$ in contrast to $\ln(R_0^2/Re)$ in (3.53). In the work of Häber *et al.* (2017), the rate of heat loss is approximated by $\lambda_g(T_s - T_\infty)/\delta_T$, which underestimates the temperature inhomogeneity during ignition and thus results in a lower critical ignition temperature.

Rewriting (3.57) in an alternative form

$$\frac{T_a}{T_{ig,cr}} \approx \ln \frac{2\nu_g B T_{ad} R_0}{\alpha_g T_a \alpha_T^2 U_\infty}, \tag{3.58}$$

we obtain that $T_a/T_{ig,cr} \propto \ln(R_0/U_\infty)$, which agrees well with the scaling relation given by Laurendeau (1982) for ignition under the condition of forced convection.

4. The effect of particle cooling on ignition

In general, ignition occurs when the heat release from chemical reaction exceeds the heat loss due to the surroundings. In addition to temperature inhomogeneity, various transient processes during the ignition process may also affect the ignition behaviour and thus modify the ignition condition, such as the drop of particle temperature and the finite residence time of the IFP staying close to the particle for $Re > 0$. In this section, we shall consider the effect of particle cooling on the ignition behaviour. The impacts of finite residence time of IFP will be discussed in the next section.

When a hot particle is in a flowing environment, heat is continuously removed from the hot particle through a combination of conduction and convection. Since the thermal conductivity of a solid is substantially greater than that of a gas, the particle temperature can be considered uniform prior to ignition. Accordingly, the energy equation for the solid

particle is given by

$$\frac{\mathrm{d}T_s}{\mathrm{d}t} = \frac{1}{\rho_s c_{vs} V_s} \int \lambda_g \left(\frac{\mathrm{d}T}{\mathrm{d}r}\right)_{r=R_0} \mathrm{d}A_s, \tag{4.1}$$

where ρ_s, c_{vs} and V_s are, respectively, the density, heat capacity and volume of the particle and A_s is the area of the particle surface. The integration on the right-hand side represents heat conduction over the particle surface. The Nusselt number representing the dimensionless total heat transfer rate is usually defined in the following general form (Leal 2007):

$$Nu \equiv -\frac{2R_0}{A_s \lambda_g (T_s - T_\infty)} \int \lambda_g \left(\frac{\mathrm{d}T}{\mathrm{d}r}\right)_{r=R_0} \mathrm{d}A_s. \tag{4.2}$$

In terms of Nusselt number, the energy equation for the spherical particle can be written as

$$\frac{\mathrm{d}T_s}{\mathrm{d}t} = -\frac{3\alpha_g \rho_g c_{pg} Nu}{2\rho_s c_{vs} R_0^2}(T_s - T_\infty). \tag{4.3}$$

When the Nusselt number is assumed to be constant, the above equation can be integrated and we obtain the following expression for the temporal change of particle temperature:

$$T_s = T_\infty + (T_{s0} - T_\infty) \exp\left(-\frac{3Nu\rho_g c_{pg} \alpha_g t}{2\rho_s c_{vs} R_0^2}\right), \tag{4.4}$$

where T_{s0} is the initial temperature of the hot particle.

According to the thermal ignition theory (Vázquez-Espí & Liñán 2001, 2002), relatively small temperature variation (of $O(T_s/T_a)$) may lead to substantial change (of $O(1)$) in the chemical reaction rate. From (4.4), the time required for the particle temperature to drop from T_{s0} to $T_{s0}(1 - T_{s0}/T_a)$ is

$$\tau_{pc} = \frac{2\rho_s c_{vs} R_0^2 T_{s0}^2}{3Nu\rho_g c_{pg} \alpha_g T_a (T_{s0} - T_\infty)}, \tag{4.5}$$

which is the characteristic time for particle cooling.

For given initial particle temperature T_{s0}, the non-dimensional heat loss coefficient $\tilde{h}$ is determined by (2.13) and the non-adiabatic ignition delay time is given by (2.16). For $\tilde{h}$ slightly smaller than e, the integral on the right-hand side of (2.16) would be of $O(1)$. For simplicity, we may use τ_{ch} given by (2.5) to represent the characteristic time for chemical reaction. Evaluating τ_{ch} by setting $T_s = T_{s0}$ in (2.5) and expressing the reaction frequency factor B in terms of the reduced Damköhler number Δ_I given by (2.2), we obtain the ratio between characteristic time for particle cooling and that for chemical reaction time

$$\frac{\tau_{pc}}{\tau_{ch}} = \frac{\rho_s c_{vs} \Delta_I T_a (1 - T_\infty/T_{s0})}{3Nu\rho_g c_{pg} T_{s0}} \left(\frac{\mathrm{d}\theta}{\mathrm{d}\tilde{r}}\right)_{\tilde{r}=1}^2. \tag{4.6}$$

Near the critical ignition state, we may analyse the order of magnitude of each term on the right-hand side of (4.4), yielding that $\Delta_I \sim O(1)$, $(T_{s0} - T_\infty)/T_{s0} \sim O(1)$,

$(\mathrm{d}\theta/\mathrm{d}\tilde{r})_{\tilde{r}=1} \sim Nu$ and $(c_{vs}/c_{pg})(T_a/T_{s0}) \sim O(1)$ for most solid particles. Consequently, the ratio τ_{pc}/τ_{ch} can be evaluated as

$$\frac{\tau_{pc}}{\tau_{ch}} \sim \frac{\rho_s}{\rho_g Nu}, \tag{4.7}$$

which is of $O(10^3)$ for most solid materials at moderate Nusselt numbers. Despite the fact that the non-adiabatic ignition delay time τ_{ig} tends to be higher than τ_{ch}, the value of the integral on the right-hand side of (2.16) may not be as large as ρ_s/ρ_g. Therefore, we have $\tau_{pc} \gg \tau_{ch}$, which indicates that the change of particle temperature is negligible during the ignition process. Consequently, the particle temperature T_s can be assumed to be constant. This assumption is used § 3.

Despite the fact that the time scale ratio scale depends on the particle radius by following $\tau_{pc}/\tau_{ch} \sim R_0^{1/2}$, it is noted that the magnitude of the ratio τ_{pc}/τ_{ch} changes slightly because of the significant density difference. Therefore, we can always have $\tau_{pc} \gg \tau_{ch}$, which can be understood as follows. On the one hand, the total thermal energy of the particle is proportional to the volume, while the heat transfer occurs on the particle surface. The relatively large surface-to-volume ratio for a small particle tends to increase the cooling rate. On the other hand, according to (3.53), the critical ignition temperature for the particle increases rapidly as the particle radius decreases. Meanwhile, the reaction rate grows exponentially with the particle temperature according to (2.5), and exceeds the increasing cooling rate due to shrinking of the particle size. In general, we conclude that the particle temperature change is not important during the ignition process, and the assumption of a constant particle temperature before ignition is validated.

5. The effect of finite residence time of IFP on ignition

In the preceding analysis, we determine the critical ignition temperature by equating the heat loss coefficient to its maximum value, i.e. $\tilde{h} = e$, which implies that the ignition delay time is infinitely large. Since ignition occurs slightly away from the particle surface, uniform flow of the reactant mixture suggests that the IFP has a finite residence time, denoted by τ_{res}, as it moves around the hot particle. Consequently, the critical ignition condition should be revised to $\tau_{res} = \tau_{ig}$.

Since the IFP must be located within the thermal boundary layer, its velocity, denoted by u_{IFP}, depends on the transverse distance from the hot particle. The largest speed of the IFP is $\tilde{u}_{\phi,\tilde{r}=1}$ of the potential flow, given by (3.17*a*,*b*). In such a situation, the arrival time of the IFP at polar angle ϕ can be calculated as

$$\tau_\phi = \frac{R_0}{U_\infty}\int_0^\phi \frac{\mathrm{d}\phi'}{\tilde{u}_{\phi,\tilde{r}=1}} \to \frac{2R_0}{3U_\infty}\left[\left(\ln\left|\tan\frac{\phi'}{2}\right|\right)_0^\phi\right]. \tag{5.1}$$

The evaluation of the integral on the right-hand side requires discussion in depth. On the one hand, for $\phi = 0$, we should have $\tau_\phi = 0$ according to the definition of integration. On the other hand, the integrand in (5.1) becomes divergent at $\phi = 0$, i.e. $\lim_{\theta\to 0} \ln|\tan\theta/2| \to \infty$. This is because both $\tilde{u}_\phi$ and $\mathrm{d}p/\mathrm{d}\theta$ vanish simultaneously at the front stagnation point according to (3.17*a*,*b*) and (3.21), i.e. there is no impetus for the fluid element to move downstream. Consequently, the residence time τ_{res} cannot be calculated by direct integration.

Due to unavoidable flow perturbations, it would be very likely that the IFP confronts the hot particle with an impact parameter, which may be arbitrarily small and which

indicates the deviation of the IFP from the stagnation point. Therefore, it is plausible to retain the condition that $\tau_\phi = 0$ for $\phi = 0$, as suggested by Coronel (2016). Then the analytical expression for τ_ϕ, represented by the last term on the right-hand side of the arrow symbol in (5.1), should be slightly revised by adding a unit within the logarithmic operator, as suggested by Coronel (2016). Accordingly, characteristic time for the potential flow moving from the front stagnation point to the separation point can be evaluated as

$$\tau_{sep} \approx \frac{2R_0}{3U_\infty} \ln \left| 1 + \tan \frac{\phi_{sep}}{2} \right|. \tag{5.2}$$

Nevertheless, equating u_{IFE} to the tangential component of the potential flow, i.e. $u_{IFP} = \tilde{u}_{\phi,\tilde{r}=1} = (3/2)\sin\phi$, considerably underestimates the residence time of the IFP and may lead to overestimation in the critical ignition temperature.

For large activation temperature, $T_a \gg T_s$, asymptotic analysis shows that intensive chemical reaction is concentrated in a relatively small region, known as Frank–Kamenetskii region (Vázquez-Espí & Liñán 2001, 2002). In the Frank–Kamenetskii region, the temperature falls from the peak value to the Frank–Kamenetskii temperature, denoted by T_{FK}, which is lower than T_{max} by an $O(\epsilon)$ with $\epsilon = T_s^2/T_a(T_{ad} - T_\infty)$. In our problem, the maximum temperature is T_s on the particle surface and for each T_s the value of ϵ can be determined uniquely, for instance, ϵ increases from 0.05 to 0.1 as particle temperature changes from 1500 to 2200 K and, for convenience, we may specify $\epsilon = 0.1$ and thus determine the normalized Frank–Kamenetskii as $\theta_{FK} = 1 - \epsilon = 0.9$ in the subsequent discussions.

The thermal boundary layer accounts for the transition of the temperature from $\theta = 1$ on the particle surface to $\theta = 0$ at the far field. The transverse coordinate corresponding to $\theta = \theta_{FK}$ defines the outer edge of the Frank–Kamenetskii region, denoted by Y_{FK}. According to Vázquez-Espí & Liñán (2001, 2002), ignition occurs within the Frank–Kamenetskii region, where the IFP must be situated. We assume that the IFP parcel is located at the edge of the Frank–Kamenetskii region and thereby define its moving velocity based on the boundary layer solution. This assumption is based on the fact that, for a fluid parcel outside the Frank–Kamenetskii region, the local reaction rate is so low that ignition can never occur during its passage across the particle. The tangential velocity of the IFP thus defined, i.e. $u_{FK} = u(\phi, Y_{FK})$, provides the upper limit describing the effects of finite residence time of IFP on the ignition behaviour and the critical ignition condition. The value of u_{FK} can be expressed in series form according to (3.23)

$$u_{FK} = F_1'(Y_{FK})\phi + F_3'(Y_{FK})\phi^3 + F_5'(Y_{FK})\phi^5 + F_7'(Y_{FK})\phi^7. \tag{5.3}$$

Figure 7 shows that the outer edge of the Frank–Kamenetskii region is slightly above the particle. From the front stagnation position to the separation point, we may approximately have $Y_{FK}/\delta_m \sim 0.1$, which is consistent with previous studies (Coronel 2016; Coronel *et al.* 2018). Consequently, the magnitude of u_{FK} at $Y = Y_{FK}$ is one order lower than $\tilde{u}_{\phi,\tilde{r}=1}$ of the potential flow.

For convenience, we may approximately correlate u_{FK} to $\tilde{u}_{\phi,\tilde{r}=1}$ through a linear relation,

$$u_{FK} = \alpha_{FK}\tilde{u}_{\phi,\tilde{r}=1} = \tfrac{3}{2}\alpha_{FK}\sin\phi, \tag{5.4}$$

where the numerical value of the proportional factor α_{FK} can be calculated by means of the series solution of the tangential velocity in the momentum boundary layer, giving

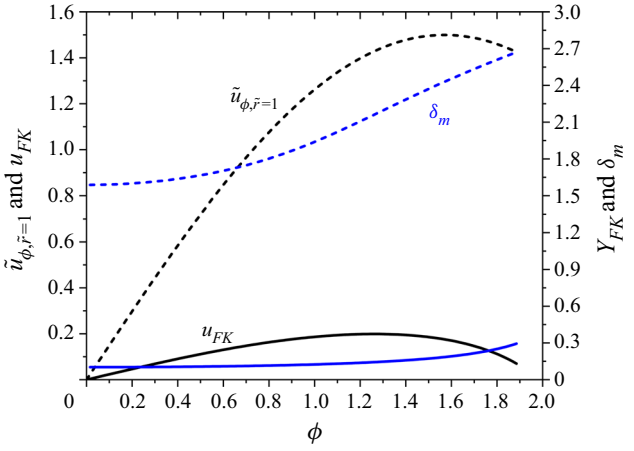

Figure 7. The blue and black solid lines respectively give the variation of Frank–Kamenetskii region thickness Y_{FK}, corresponding to $\theta_{FK} = 0.9$, and the tangential velocity component u_{FK} at that distance. The blue and black dashed lines provide the boundary layer thickness δ_m and the tangential component of the potential velocity for comparison.

$\alpha_{FK} \approx 0.15$. Replacing $\tilde{u}_{\phi,\tilde{r}=1}$ by u_{FK} in (5.1) provides the correction of the residence time for IFP, i.e.

$$\tau_{res} = \frac{2R_0}{3U_\infty \alpha_{FK}} \ln\left|1 + \tan\frac{\phi_{sep}}{2}\right|. \tag{5.5}$$

According to (5.5) and (5.2), we have $\tau_{res}/\tau_{sep} = 1/\alpha_{FK}$, which is considerably greater than unity. This demonstrates that the residence time of the IFP should not be evaluated by the characteristic time for potential flow past a spherical particle.

Equating τ_{res} in (5.5) to the ignition delay time τ_{ig} calculated via (2.16), we revise the ignition criterion by considering the motion of the IFP and thereby determine the critical ignition temperature.

To derive an explicit formula for T_{cr}, the integral on the right-hand side of (2.16), which is defined as a function of $\tilde{h}$,

$$F_{ig}(\tilde{h}) = \int_0^\infty \frac{\mathrm{d}\chi}{e^\chi - \tilde{h}\chi}, \tag{5.6}$$

must be evaluated in analytical sense. Here, F_{ig} can be understood as the amplifying factor of ignition delay in the presence of heat loss. The series of F_{ig} in powers of $\tilde{h}$ converges very slowly. To reproduce the asymptotic behaviour of $F_{ig} \to \infty$ as $\tilde{h} \to e$, one has to retain terms of $\tilde{h}^{100}$, and thus the series exhibits little applicability in analytical operations. However, the general behaviour of $F_{ig}(\tilde{h})$ suggests that we may approximately evaluate its value through a simplified model in the subsequent form

$$F'_{ig}(\tilde{h}) = \frac{1}{1 - \tilde{h}/e}. \tag{5.7}$$

The model F'_{ig} is consistent with F_{ig} satisfying that $F'_{ig}(0) = F_{ig}(0) = 1$ and the asymptotic behaviour that $F'_{ig} \to \infty$ as $\tilde{h} \to e$. Figure 8 shows that, in almost the whole range of $\tilde{h}$, the relative deviation between F'_{ig} and F_{ig}, defined by $f_{err} = |F_{ig} - F'_{ig}|/F_{ig}$,

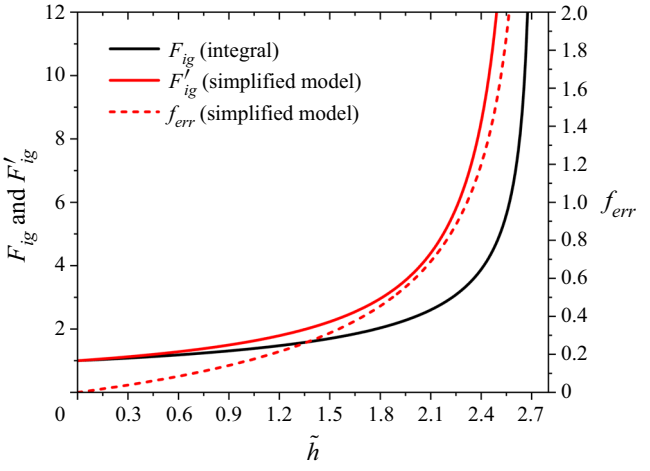

Figure 8. Comparison of F'_{ig} predicted by simplified model (5.7) with F_{ig} calculated by integral (5.6). The solid lines represent the variation of F_{ig} or F'_{ig} with the non-dimensional heat loss coefficient, whose deviations f_{err} are indicated by the dashed lines.

is of $O(1)$, suggesting qualitative agreement between the simplified model F'_{ig} and the exact integral F_{ig}. Replacing F_{ig} by F'_{ig} enables solution of $\tilde{h}$ (or equivalently T_s) with knowledge of τ_{ig} (or equivalently τ_{res}) and hence provides convenience in deriving an explicit expression for T_{cr}.

Using the simplified model F'_{ig} in the ignition criterion $\tau_{res} = \tau_{ig}$, we obtain

$$\frac{T_a}{T_{ig,cr}} = \ln \frac{2T_{ad}(1 - T_\infty/T_{ad})BR_0^2}{T_a(1 - T_\infty/T_{ig,cr})^2\alpha_g} - 2\ln(1 + \alpha_T Re^{1/2}) - \ln\left[1 + \frac{3\alpha_{FK}Pe}{Ar^2 \ln|1 + \tan(\phi_{sep}/2)|(1 + \alpha_T Re^{1/2})^2}\right], \tag{5.8}$$

where $Ar = T_a/T_{ig,cr}$ is the Arrhenius number and is usually of $O(10)$.

The first and second terms on the right-hand side of (5.8) are identical to those in (3.53), which interprets the effect of temperature inhomogeneity, resulting from respectively conductive and convective heat transfer, on the critical ignition temperature. The additional growth of T_{cr} due to the motion of IFP is represented by the last term on the right-hand side of (5.8), which vanishes identically by either taking $\alpha_{FK} = 0$ (i.e. IFP attached to the particle surface) or $Pe = 0$ (i.e. the combustible mixture in a quiescent condition). The magnitude of this additional term appears to be considerably smaller than the remaining terms, which implies that the motion of the IFP can hardly contribute to the elevation of $T_{ig,cr}$.

Figure 9 shows the change of critical ignition temperature, corresponding to a spherical particle of radius 0.4 mm in a stoichiometric CH_4/air mixture, with uniform flow velocity. It is observed that the discrepancies between the solid lines appears to be indiscernible, which demonstrates that considering the motion of the IFP results in negligible change in the critical ignition temperature. Replacing F_{ig} by its simplified model F'_{ig} results in the elevation of $T_{ig,cr}$, as indicated by the difference between the blue and red lines of either solid or dashed type in figure 9. This can be attributed to the fact that the

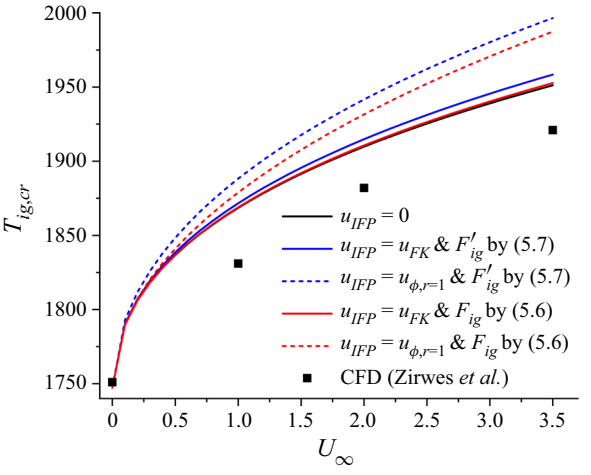

Figure 9. The variation of critical ignition temperature with uniform flow velocity, where the motion of the IFP is taken into account. The black/red/blue solid lines refer to theoretically predicted $T_{ig,cr}$ respectively by (3.53) without motion of the IFP, by revised criterion $\tau_{res} = \tau_{ig}$ equating $u_{IFP} = u_{FK}$ with F_{ig} calculated based on its definition, i.e. (5.6), and with F'_{ig} evaluated through the simplified model, i.e. (5.7). The dashed lines denote $T_{ig,cr}$ values obtained by the revised criterion $\tau_{res} = \tau_{ig}$ corresponding to underestimated residence time with $u_{IFE} = \tilde{u}_{\phi,\tilde{r}=1}$. The symbols denote results from simulation (Zirwes *et al.* 2019).

magnitude of F'_{ig} is uniformly higher than that of F_{ig} in the whole range of $\tilde{h}$, as shown in figure 8, and thereby overestimates the heat loss effect during ignition. Nevertheless, quantitative interpretation of the critical ignition condition requires appropriate evaluation of the velocity of the IFP, u_{IFP}. Comparison between the solid and dashed lines in figure 9 indicates that equating u_{IFP} to $u_{\phi,\tilde{r}=1}$ outside the boundary layer would lead to a physically implausible boost in $T_{ig,cr}$. This can be attributed to the considerable reduction of the residence time of the IFP, which is equivalent to an intensification of the heat loss effect during the ignition process. Besides, the fact that the temperature of the IFP is close to T_s denies the specification of $u_{IFP} = u_{\phi,\tilde{r}=1}$ because the temperature at the outer edge of the boundary can never be close to T_s and thereby hardly support a rapid chemical reaction.

6. Conclusions

In this work, we conducted theoretical analysis on the inhomogeneous ignition of a combustible mixture by a hot particle. We revised Semenov's transient ignition criterion by introducing a hypothetical volumetric heat loss coefficient that accounts for the actual temperature inhomogeneity. The revised ignition criterion allows us to determine the critical ignition temperature. The critical ignition temperature is primarily determined by the temperature inhomogeneity, which is quantified by the temperature gradient on the particle surface and depends on the relative motion between the hot particle and the ambient gas. At quiescent conditions with $Re = 0$, the temperature inhomogeneity is caused by pure heat conduction and is dominantly affected by particle size, yielding the result that the critical ignition temperature grows noticeably as the particle radius decreases. At conditions of $Re \ll 1$, the creeping flow of the combustible mixture tends to accumulate thermal energy on the rear hemisphere, which leads to non-uniformity of the temperature gradient and thus facilitates ignition at the rear stagnation point. As Re continuously increase, flow separation originates from the rear stagnation point and moves

upstream. The momentum and thermal boundary layers before the separation point were solved using a Blasius series, and the temperature gradient was obtained. Defining the temperature gradient for ignition, i.e. lowest $(\partial\theta/\partial\tilde{r})_{\tilde{r}}$ over the particle surface, we derived an explicit formula that correlates the critical ignition temperature with the temperature inhomogeneity and the properties of the flammable mixture relating to its chemical reactivity and molecular transport. The formula can be used to individually quantify the contributions of various transient effects.

Due to the exceedingly large density ratio between the particle and the ambient gas, the unsteadiness of particle cooling due to continuous heat transfer to the combustible mixture was shown to make a negligible contribution to the ignition process. Besides, the finite residence time of the IFP was considered and evaluated in the Frank–Kamenetskii region. The theoretical formula for the critical ignition temperature was revised to include an additional term accounting for the transient effect of a finite residence time of the IFP.

In general, the critical ignition temperature predicted by the present theory agrees well with those obtained in experiments and numerical simulations for methane/air and hydrogen/air mixtures. The discrepancy in quiescent situations can be attributed to the fact that the frequency factor B is evaluated based on relevant data at high temperature and thus overestimates the reaction rate in the low-temperature regime. A revised Arrhenius-type reaction rate model considering the temperature dependence of the pre-exponential factor would improve the theoretical prediction of the critical ignition temperature. In the presence of relative motion between the particle and the ambient gas, the discrepancy in the critical ignition temperature can be attributed to the assumption of constant transport properties. In the present analysis, the viscosity of the ambient premixture is evaluated at the environmental temperature, resulting in overestimation of the Reynolds number. Accordingly, the stronger temperature inhomogeneity at the ignition location corresponds to a higher critical ignition temperature. However, when the temperature dependence of the transport properties is considered, the energy equation for the ambient premixture becomes nonlinear and an analytical solution cannot be obtained.

This work neglects the thermal expansion of the ambient premixture and the radiative heat transfer from the particle. For a particle of sufficiently high temperature, thermal expansion may alter the flow field close to the particle surface, which in turn affects the heat transfer rate and thereby the critical ignition temperature. The thermal radiation of the hot particle may provide an additional route to the heating of the flammable mixture, and the additional time scale for radiative heat transfer may also change the critical ignition temperature. Besides, radical destruction reactions may take place on the particle surface, which modify the local temperature profile and consequently may affect the ignition behaviour. In future works, it would be interesting to take into account these effects. It would be exceedingly difficult to deal with these effects in a theoretical analysis, and thereby numerical simulations maybe conducted instead.

Funding. This work was supported by National Natural Science Foundation of China under Grant Nos. 52006001 and 52176096, and by Opening Fund of State Key Laboratory of Fire Science (SKLFS) under Grant No. HZ2021-KF01.

Declaration of interests. The authors declare no conflict of interest.

Author ORCIDs.
Dehai Yu https://orcid.org/0000-0002-6950-777X;
Zheng Chen https://orcid.org/0000-0001-7341-6099.

References

Beyer, M. & Markus, D. 2012 Ignition of explosive atmospheres by small hot particles: comparison of experiments and simulations. *Sci. Technol. Energetic Mater.* **73**, 1–7.

Coronel, S.A. 2016 *Thermal Ignition using Moving Hot Particles*. PhD Thesis, California Institute of Technology.

Coronel, S.A., Melguizo-Gavilanes, J., Mével, R. & Shepherd, J.E. 2018 Experimental and numerical study on moving hot particle ignition. *Combust. Flame* **192**, 495–506.

Eckhoff, R.K. & Thomassen, O. 1994 Possible sources of ignition of potential explosive gas atmospheres on offshore process installations. *J. Loss Prev. Process Ind.* **7**, 281–294.

Glassman, I., Yetter, R.A. & Glumac, N.G. 2014 *Combustion*. Academic Press.

Häber, T., Zirwes, T., Roth, D., Zhang, F., Bockhorn, H. & Maas, U. 2017 Numerical simulation of the ignition of fuel/air gas mixtures around small hot particles. *Z. Phys. Chem.* **231**, 1625–1654.

Hawksworth, S., Rogers, R., Proust, C., Beyer, M., Schenk, S., *et al.* 2005 Ignition of explosive atmospheres by mechanical equipment. *Hazards* **18**, 23–25.

Hughmark, G. 1980 Heat and mass transfer for spherical particles in a fluid field. *Ind. Engng Chem. Fundam.* **19**, 198–201.

Johnson, T. & Patel, V. 1999 Flow past a sphere up to a Reynolds number of 300. *J. Fluid Mech.* **378**, 19–70.

Landau, L. & Lifshitz, E. 1987 Theoretical physics. In *Fluid Mechanics*, vol. 6. Pergamon.

Laurendeau, N.M. 1982 Thermal ignition of methane air mixtures by hot surfaces: a critical examination. *Combust. Flame* **46**, 29–49.

Law, C.K. 1978*a* Ignition of a combustible mixture by a hot particle. *AIAA J.* **16**, 628–630.

Law, C.K. 1978*b* On the stagnation-point ignition of a premixed combustible. *Intl J. Heat Mass Transfer* **21**, 1363–1368.

Law, C.K. 1979 Transient ignition of a combustible by stationary isothermal bodies. *Combust. Sci. Technol.* **19**, 237–242.

Law, C.K. 2010 *Combustion Physics*. Cambridge University Press.

Leal, L.G. 2007 *Advanced Transport Phenomena: Fluid Mechanics and Convective Transport Processes*. Cambridge University Press.

McAllister, S., Chen, J.-Y. & Fernandez-Pello, A.C. 2011 *Fundamentals of Combustion Processes*. Springer.

Melguizo-Gavilanes, J., Coronel, S., Mével, R. & Shepherd, J. 2017*a* Dynamics of ignition of stoichiometric hydrogen-air mixtures by moving heated particles. *Intl J. Hydrog. Energy* **42**, 7380–7392.

Melguizo-Gavilanes, J., Mével, R., Coronel, S. & Shepherd, J. 2017*b* Effects of differential diffusion on ignition of stoichiometric hydrogen-air by moving hot spheres. *Proc. Combust. Inst.* **36**, 1155–1163.

Melguizo-Gavilanes, J., Nové-Josserand, A., Coronel, S., Mével, R. & Shepherd, J.E. 2016 Hot surface ignition of n-hexane mixtures using simplified kinetics. *Combust. Sci. Technol.* **188**, 2060–2076.

Mével, R., Melguizo-Gavilanes, J., Boeck, L. & Shepherd, J. 2019 Experimental and numerical study of the ignition of hydrogen-air mixtures by a localized stationary hot surface. *Intl J. Heat Fluid Flow* **76**, 154–169.

Mével, R., Niedzielska, U., Melguizo-Gavilanes, J., Coronel, S. & Shepherd, J.E. 2016 Chemical kinetics of *n*-hexane-air atmospheres in the boundary layer of a moving hot sphere. *Combust. Sci. Technol.* **188** (11–12), 2267–2283.

Paterson, W. & Hayhurst, A. 2000 Mass or heat transfer from a sphere to a flowing fluid. *Chem. Engng Sci.* **55**, 1925–1927.

Proust, C., Hawksworth, S., Rogers, R., Beyer, M., Lakic, D., *et al.* 2007 Development of a method for predicting the ignition of explosive atmospheres by mechanical friction and impacts (MECHEX). *J. Loss Prev. Process Ind.* **20**, 349–365.

Riley, N. 1986 The heat transfer from a sphere in free convective flow. *Comput. Fluids* **14**, 225–237.

Rimon, Y. & Cheng, S. 1969 Numerical solution of a uniform flow over a sphere at intermediate Reynolds numbers. *Phys. Fluids* **12**, 949–959.

Roth, D., Häber, T. & Bockhorn, H. 2017 Experimental and numerical study on the ignition of fuel/air mixtures at laser heated silicon nitride particles. *Proc. Combust. Inst.* **36**, 1475–1484.

Roth, D., Sharma, P., Haeber, T., Schiessl, R., Bockhorn, H. & Maas, U. 2014 Ignition by mechanical sparks: ignition of hydrogen/air mixtures by submillimeter-sized hot particles. *Combust. Sci. Technol.* **186**, 1606–1617.

Schlichting, H. & Gersten, K. 2016 *Boundary-Layer Theory*. Springer.

STAMATOV, V., KING, K. & ZHANG, D. 2005 Explosions of methane/air mixtures induced by radiation-heated large inert particles. *Fuel* **84**, 2086–2092.

SU, Y., HOMAN, H. & SIRIGNANO, W. 1979 Numerical predictions of conditions for ignition of a combustible gas by a hot, inert particle. *Combust. Sci. Technol.* **21**, 65–74.

SU, Y.-P. & SIRIGNANO, W. 1981 *Symposium (International) on Combustion 1981*, vol. 18, pp. 1719–1728. Elsevier.

URBAN, J.L. 2017 *Spot Ignition of Natural Fuels by Hot Metal Particles*. University of California.

URBAN, J.L., ZAK, C.D., SONG, J. & FERNANDEZ-PELLO, C. 2017 Smoldering spot ignition of natural fuels by a hot metal particle. *Proc. Combust. Inst.* **36**, 3211–3218.

VÁZQUEZ-ESPÍ, C. & LIÑÁN, A. 2001 Fast, non-diffusive ignition of a gaseous reacting mixture subject to a point energy source. *Combust. Theory Model* **5**, 485–498.

VÁZQUEZ-ESPÍ, C. & LIÑÁN, A. 2002 Thermal-diffusive ignition and flame initiation by a local energy source. *Combust. Theory Model* **6**, 297.

WANG, Y. & CHEN, Z. 2020 Effects of particle size on the ignition of static CH4/air and H2/air mixtures by hot particles. *Combust. Sci. Technol.* doi:10.1080/00102202.2020.1788006.

WANG, S., HUANG, X., CHEN, H. & LIU, N. 2016 Interaction between flaming and smouldering in hot-particle ignition of forest fuels and effects of moisture and wind. *Intl J. Wildland Fire* **26**, 71–81.

WANG, Y., ZHANG, H., ZIRWES, T., ZHANG, F., BOCKHORN, H. & CHEN, Z. 2021 Ignition of dimethyl ether/air mixtures by hot particles: impact of low temperature chemical reactions. *Proc. Combust. Inst.* **38**, 2459–2466.

ZIRWES, T., ZHANG, F., HÄBER, T. & BOCKHORN, H. 2019 Ignition of combustible mixtures by hot particles at varying relative speeds. *Combust. Sci. Technol.* **191**, 178–195.